SARS-CoV-2 proteins bind heme and hemoglobin.

Guilherme Curty Lechuga[1,2*], Franklin Souza-Silva[1,3*], Carolina de Queiroz Sacramento[1,4], Monique Ramos de Oliveira Trugilho[1,5], Richard Hemmi Valente[5], Paloma Napoleão-Pêgo[1], Suelen da Silva Gomes Dias[4], Natalia Fintelman-Rodrigues[1,4], Jairo Ramos Temerozzo[1,4], Nicolas Carels[1,3], Carlos Roberto Alves[6], Mirian Claudia de Souza Pereira[2], David William Provance, Jr[1], Thiago Moreno Lopez Souza[1,4], Salvatore Giovanni De-Simone[1,7,**]

[1]FIOCRUZ, Center of Technological Development in Health (CDTS)/National Institute of Science and Technology for Innovation on Neglected Population Diseases (INCT-IDPN), Rio de Janeiro, RJ, Brazil;
[2]FIOCRUZ, Oswaldo Cruz Institute, Celular Ultrastructure Laboratory, Rio de Janeiro, RJ, Brazil;
[3]Iguaçu University, Nova Iguaçu, RJ, Brasil;
[4]FIOCRUZ, Oswaldo Cruz Institute, Immunopharmacology Laboratory, Rio de Janeiro, RJ, Brazil.
[5]FIOCRUZ, Oswaldo Cruz Institute, Laboratory of Toxinology, Rio de Janeiro, RJ, Brazil;
[6]FIOCRUZ, Oswaldo Cruz Institute, Molecular Biology and Endemic Diseases Laboratory, Rio de Janeiro, RJ, Brasil;
[7]Federal Fluminense University, Biology Institute, Department of Cellular and Molecular Biology, Niterói, RJ, Brazil.

[*]**These authors contributed equally to this work**
[**]**Corresponding author:** FIOCRUZ, CDTS, Pav. Leonidas Deane, room 309, Av. Brasil 4365, 21040-900, Rio de Janeiro, RJ, Brazil. *E-mail*. **dsimone@cdts. fiocruz.br** (De-Simone SG)

Keywords: Sars-CoV-2, Covid-19, Heme, Hemoglobin, binding protein

Abstract

The coronavirus disease 2019 (COVID-19) pandemic, caused by severe acute respiratory syndrome virus 2 (SARS-CoV-2), has led to a global crisis that included collapsing healthcare systems and shut-down communities, producing considerable economic burden. Despite the number of effective vaccines quickly implemented, the emergence of new variants is a primary concern. The scientific community undertook a rapid response to better study this new virus. However, critical questions about viral protein-protein interactions and mechanisms of its physiopathology are still unclear. Although severe COVID-19 was associated with hematological dysfunctions, scarce experimental data were produced about iron dysmetabolism and the viral proteins' possible interaction with hemoglobin (Hb) chains. This work demonstrates the binding of SARS-CoV-2 proteins to hemin and Hb using a multimethodological approach. *In silico* analysis indicated binding motifs between a cavity in the viral nucleoprotein and hemoglobin's porphyrin coordination region. Different hemin binding capacities of mock and SARS-CoV-2-infected culture extracts were noticed using gel electrophoresis and TMB staining. Hemin-binding proteins were isolated from SARS-CoV-2-infected cells by affinity chromatography and identified by shotgun proteomics, indicating that structural (nucleoprotein, spike, and membrane protein) and non-structural (Nsp3 and Nsp7) viral proteins interact with hemin. *In vitro* analyses of virus adsorption to host cells

and viral replication studies in Vero cells demonstrated inhibitory activities - at different levels - by hemin, protoporphyrin IX (PpIX) Hb. Strikingly, free Hb at 1μM suppressed viral replication (99 %), and its interaction with SARS-CoV-2 was localized to the RBD region of the Spike protein. The findings showed clear evidence of new avenues to disrupt viral replication and understand virus physiopathology that warrants further investigation.

Introduction

At the end of 2019, severe acute respiratory syndrome coronavirus 2 (SARS-CoV-2) was first recognized in Wuhan (Hubei province, China). The disease rapidly spread to many countries due to its high transmissibility and prolonged incubation, allied to the existing highly connected global travel network [1]. This zoonotic virus became the etiological agent of the 2019 coronavirus disease (COVID-19). As an ongoing pandemic disease, COVID-19 has proven to be a significant economic and public health challenge. The elderly and individuals with pre-existing comorbidities are severely affected, but severe COVID-19 can impact the full range of age groups [2]. The global scientific community has exerted tremendous efforts to understand the viral structure and physiopathology to identify control measures that include drug repurposing strategies, plasmapheresis, and vaccination [3]. Despite the performance and increasing availability of the newly developed vaccines, the recent detection of emerging variants that appear to escape from the immune responses represents a significant concern to immunization strategies [4].

Although drug repurposing has not been proved to be unequivocally satisfactory against SARS-CoV-2, this strategy could still be worth fighting COVID-19 when appropriate biochemical interactions of viral proteins and small molecules are determined. Possibly, biochemically-based evidence of effective treatments for current and future variants can be accelerated by expanding the breadth of knowledge on the activities of the individual SARS-CoV-2 proteins during infection, avoiding further frustration in clinical trials with molecules with limited preclinical effectiveness against SARS-CoV-2, such as lopinavir (targeting viral protease) in combination with ritonavir (LPV/RTV), and hydroxychloroquine (HCQ) [5]. Hematological COVID-19 is a constitutive component in critically ill patients [6,7]. The heme-iron dysregulation has been observed in COVID-197, with binding signatures including hyperferritinemia, low hemoglobin (Hb) levels, low serum iron, anisocytosis, and increased variation of red blood cell distribution width (RDW), and hypoxemia [8–10]. Unbalanced erythrocyte counts, Hb, and iron levels were associated with poor clinical outcomes in COVID-199. An *in silico* analysis pointed to a relevant role of SARS-CoV-2 proteins in viral physiopathology. The predictions suggest that the capture of heme, resulting from a coordinated attack of orf1ab, ORF10, and ORF3a to the 1-β chain of hemoglobin, could interfere with heme metabolism and oxygen transport. This analysis also proposed the binding of

heme by structural and non-structural proteins of SARS-CoV-2 [6]. Although these data bring interesting perspectives, experimental confirmation is still needed.

Heme, iron protoporphyrin IX (PpIX), is a ubiquitous molecule with importance in numerous biological processes such as a cofactor for proteins (Hb), transcriptional regulation [11], RNA processing [12], oxidative stress [13], inflammation [14], and coagulation [15], which are all critical aspects of COVID-19 pathology. Heme and porphyrins can modulate viral infection by targeting both viral structures and cellular pathways. Porphyrins have broad activities against different viruses such as hepatitis B virus (HBV), hepatitis C virus (HCV), human immunodeficiency virus (HIV), and Zika virus (ZIKV) [16,17]. Nonspecific heme interactions, including hydrophobic binding to viral surface envelope proteins, block viral cellular entry [18]. Potent antiviral activity of PpIX and verteporfin in the nanomolar range has been recently reported in the inhibition of viral invasion by blocking the virus-cell fusion mediated by SARS-CoV-2 Spike (S) protein and ACE2 [19]. When Vero cells were pretreated with both, there was an inhibition of viral RNA production, suggesting that their interactions with ACE2 caused the viral entry block.

Despite the concerted efforts to unveil key viral targets, experimental evidence is still limited. Here, we focused on the capacity of SARS-CoV-2 proteins to capture heme and Hb. Our findings demonstrate that SARS-CoV-2 structural and non-structural proteins can bind to hemin. An *in silico* analysis identified heme-binding motifs in nucleoprotein and *in vitro* assays showed that the approved drugs hemin and PpIX precluded - at different levels - viral attachment to host cells, reducing viral replication. Notably, free Hb suppressed viral entry by interaction with the RBD region in the Spike protein and reduced viral replication. The results suggest that these molecules could be promising candidates for the treatment of COVID-19 and highlight the need to investigate further the mechanisms involved with the iron dysmetabolism observed in infected individuals.

Results

In silico analysis

The mapping of the binding motifs to heme was the first step in this study's *silico* approach. Analysis of 68 crystallized hemoglobin/heme complex structures (**Supplementary Table 1**) identified conserved amino acid residues (identical in at least 97 % of the analyzed structures in the same position) that interact with the heme group. Furthermore, Histidine displayed the highest binding frequency to heme, while Alanine had the lowest contribution (**Fig. 1a**). From the mapped motifs in human hemoglobin (**Supplementary Figure 1**) three equivalent motifs in SARS-CoV-2 nucleoprotein - presenting different E-values (**Supplementary Figure 2**): motif 1 = 3.4×10^{-505}, motif 2 = 4.4×10^{-532} and motif 3 = 1.8×10^{-628} - were identified (Fig. 1b). These analyses also indicate a correspondence regarding the residues Tyr

(in motif 1), Lys (in motif 2), and Leu and Phe (in motif 3) in heme-binding motif composition between human Hb and the nucleoprotein of SARS-CoV-2 (**Fig. 1b**).

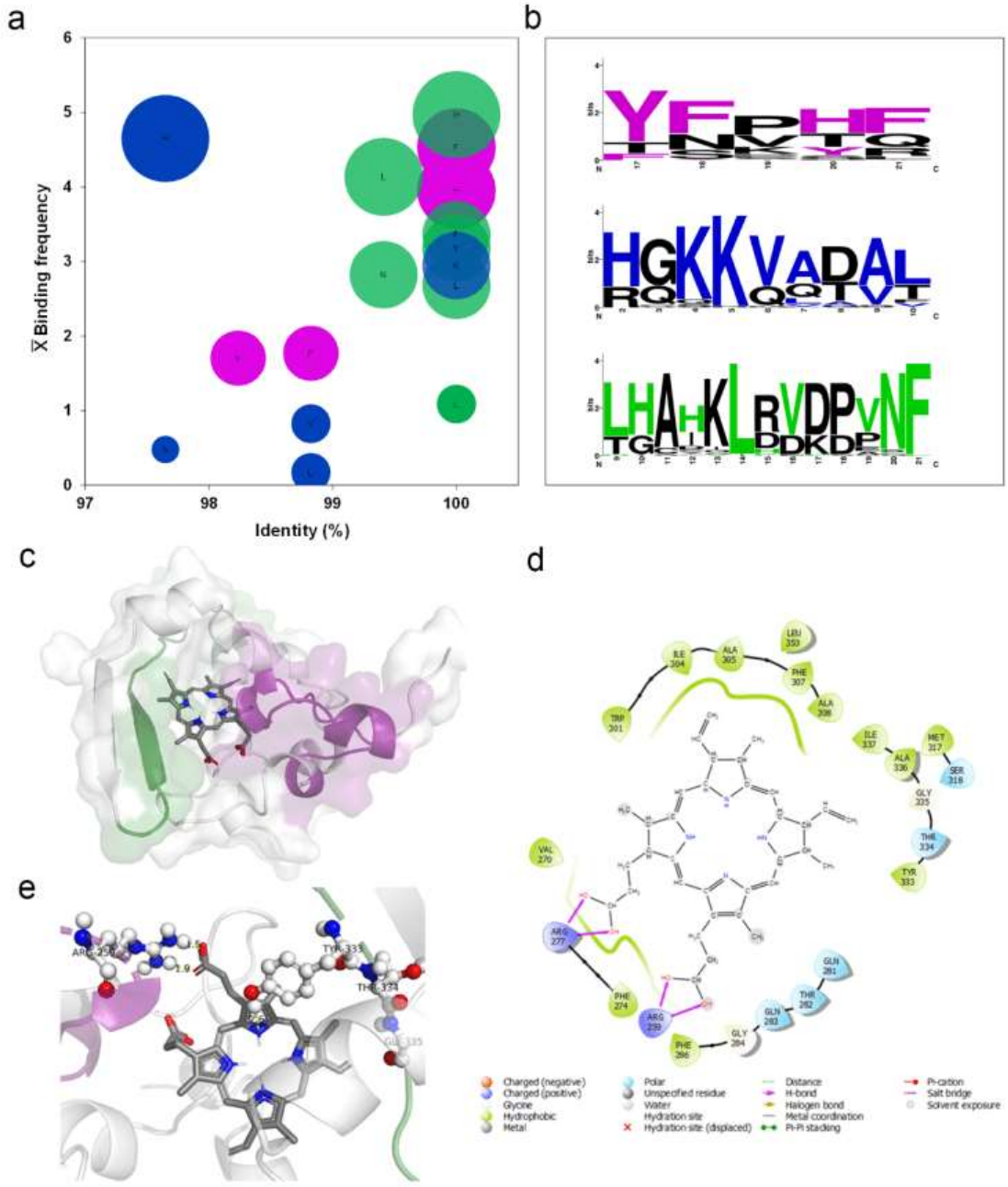

Fig. 1: Heme-binding motifs identified by an *in silico* analysis. (**a**) the heme-binding motifs for 68 Hb structures deposited in the PDB data bank were mapped to define the frequency of amino acid occurrence ($\bar{X}$ Binding frequency) and degree of identity (%). The balls' size is relative to the number of connections (5 to 1), displayed from biggest to smallest in size. (**b**) three binding motifs were identified in the nucleoprotein of SARS-CoV-2 by an analysis in the MEME-Suite server of Hb amino acid sequence obtained from Uniprot sever. Colored amino acids related to residues in Hb that interact with heme. Black residues form part of the motif without binding heme. The size of the amino acid relates to the number of occurrences (bits). Molecular docking of SARS CoV-2 nucleoprotein with human PpIX. (**c**) Binding position of PpIX (sticks) indicating the orientation of binding with nucleoprotein (surface) to predicted motifs: purple = motif 1 and green = motif 3. (**d**)

2D representation indicating types of bonds that occur in nucleoprotein pocket bounded with PpIX. (**e**) 3D model showing nucleoprotein amino acid residues (ball and sticks) that compose motifs 1 and 3 coordinating the binding with the PpIX (bars).

The molecular docking assay was initially necessary to identify possible binding pockets in the SARS-CoV-2 nucleoprotein. A cavity with a -9.8 kcal/mol binding energy and a 121 Å size was selected to be assayed. In this cavity, it was possible to identify the bonds of PpIX with motifs 1 and 3 (**Fig. 1c**), with a predominance of hydrophobic bonds followed by polar bonds and hydrogen bonds (**Fig. 1d**) with porphyrin propionate groups. Both motifs' potential to contribute to the coordination of protoporphyrin binding was related with Arg259 of motif 1 performing hydrogen bonding and Tyr333, Thr334, and Gly335 of motif 3 performing hydrophobic and polar bonds, respectively (**Fig. 1e**).

Proteins from SARS-CoV-2-infected cells extract bind to hemin (heme)

Two distinct approaches evaluated the cellular and viral proteins' interaction with heme. In the first, 300 μM hemin was pre-incubated with protein extracts obtained from Vero cell cultures, either infected with SARS-CoV-2 or mock-infected, as a control, followed by SDS-PAGE separation, in-gel protein renaturation, and heme-binding protein visualization using TMB reaction. Two protein bands (*ca.* 55 and 70 kDa) were revealed for SARS-CoV-2 infected Vero cells protein extract sample, with only a very faint band stained at ~55 kDa in the mock protein extract sample **(Fig. 2a; right side**). As expected, no bands were visualized from the oxidation of TMB oxidation for the negative control samples in the absence of hemin's addition (**Fig. 2a; left side**). The alternative approach separated protein extracts by SDS-PAGE under denaturing and reducing conditions transferred to a nitrocellulose membrane before incubation with 2 μM hemin. Bound hemin was revealed by its reaction with DAB. This approach displayed a greater sensitivity for detecting protein-heme complexes, as seen by the more significant number of visible protein bands. The patterns showed differences between the proteins' profiles that can interact with heme in uninfected and virus-infected cells. The bands previously observed by the first approach were also detected, with the band at ~55 kDa being the most prominent. Among the revealed bands, four (*ca.* 45, 55, 70, and 230 kDa) were exclusively detected in the protein extract of SARS-CoV-2-infected cells (**Fig. 2b**).

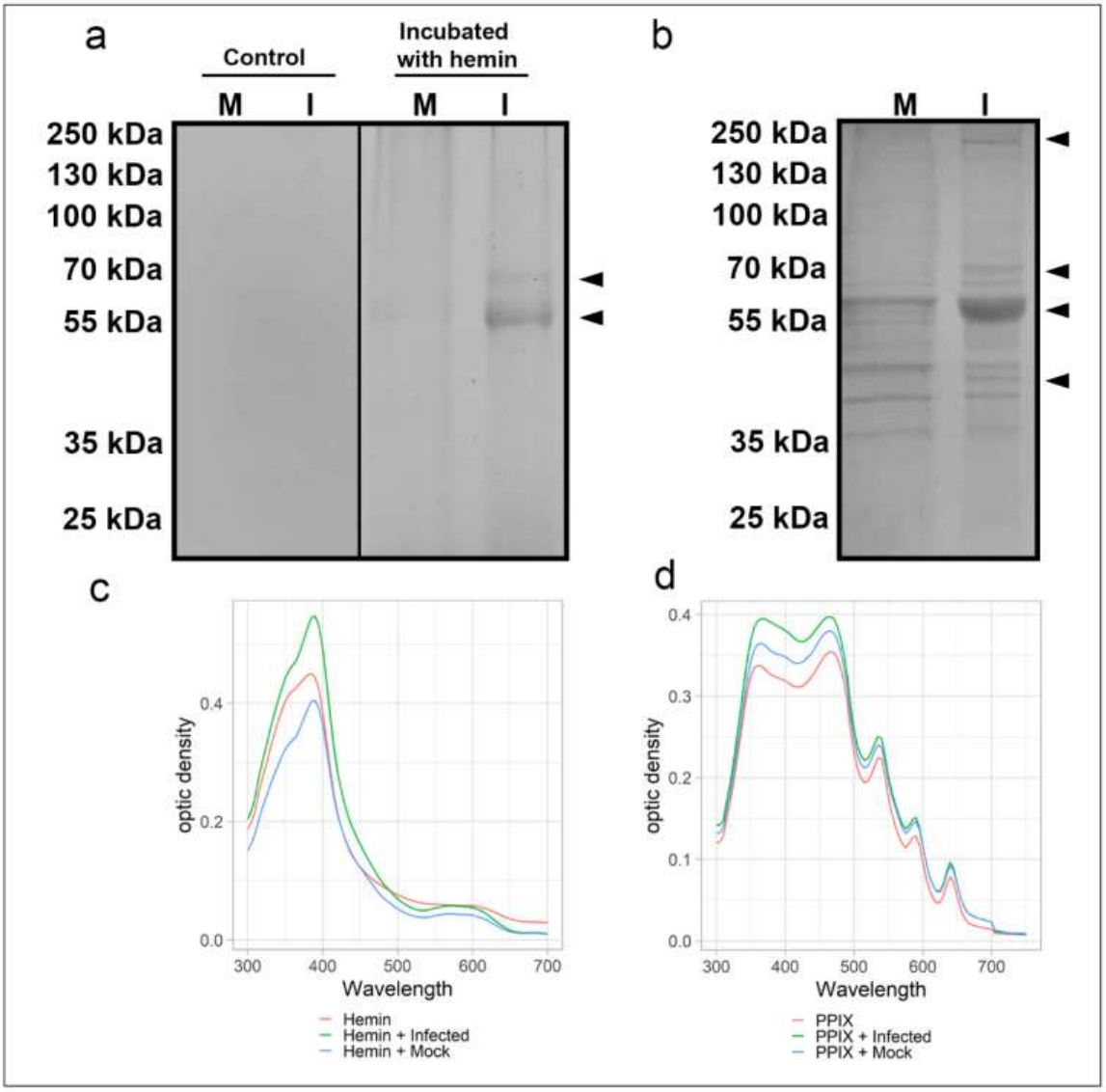

Fig. 2: Heme-binding proteins in extracts from SARS-CoV-2 infected and non-infected Vero cells along with a spectroscopic binding analysis in solution. Total protein extracts (20 μg) from virus-infected (I) and mock-infected (M) were: **a**) incubated with 300 μM of hemin for 1 h at 25 °C, separated by SDS-PAGE, renatured and exposed to TMB in-gel to reveal hemin or (**b**) resolved by SDS-PAGE, transferred to nitrocellulose membrane and incubated with hemin (2 μM) for 1 h before revealing hemin-protein complexes by DAB. Arrowheads indicate bands of hemin-protein complexes. UV-visible spectra of hemin (**c**) alone (10 μM, red) or in total protein extracts (20 μg) of virus-infected Vero cells (green) and mock-infected cells (blue). UV-visible spectra of PpIX (**d**) alone (5 μM, red) or in total protein extracts (20 μg) of virus-infected Vero cells (green) and mock-infected cells (blue). Changes in the Soret peak and Q-bands are observable. Data are representative of two independent experiments. Source data are provided as a Source Data file.

These observations of heme-binding protein in-gel and on membranes raised questions about their binding properties in solution. UV-visible spectra of hemin (10 μM) diluted in PBS were recorded to analyze possible viral protein interactions with heme, revealing a Soret peak with a lambda maximum at 385 nm. Changes in hemin absorption spectra were observed after incubation with mock and virus-

infected protein extracts. A redshift was noticed in both cellular extracts (lambda max. 390 nm) (**Fig. 2c**). Furthermore, the Soret band and protoporphyrin IX absorbance in both the Soret region and the Q bands were increased in mock and virus-infected cell extract (**Fig. 2d**).

SARS-CoV-2 proteins identification and confirmation of binding to hemin and hemoglobin

Shotgun proteomics was used to identify which SARS-CoV-2 proteins were interacting with heme. Initially, SARS-CoV-2-infected Vero cells total protein extract was subjected to SDS-PAGE separation, followed by excision of all visible bands and submission to processing for protein content identification nanoelectrospray coupled to high-resolution tandem mass spectrometry (LC-MS/MS). This approach yielded virus protein identifications in the six bands indicated in figure 3a. Nucleoprotein was identified in almost all excised bands (2, 3, 4, 5, and 6). Spike protein was identified in bands 1, 2, 3, and 6, while membrane protein was identified in bands 1 and 3. The non-structural proteins NSP3 and NSP2 were detected in bands 1 and 3, respectively (**Fig. 3a**). The most abundant protein identified in band 4 was albumin, probably due to supplementation in the culture medium. To reduce the amount of this contaminant protein that could interfere or mask the signal of viral proteins, albumin was depleted using affinity chromatography followed by hemin-agarose binding. Next, albumin-depleted protein extract of SARS-CoV-2 infected Vero cells was incubated with hemin-agarose beads to confirm that viral proteins can interact and bind heme. Finally, the hemin-agarose eluate containing the hemin-binding proteins was subjected to SDS-PAGE under denaturing and reducing conditions, revealing the presence of several viral proteins, as identified by LC-MS/MS (**Fig. 3b**). In-band 7, nucleoprotein, Spike, Nsp3, Nsp7, and membrane protein were placed. Nucleoprotein was also present in band 8 with the highest spectral counts and Spike protein in lower abundance. Additional information regarding cellular proteins and spectral counts obtained for each band can be found in the supplemental material (**Supplementary Data 1**). Additionally, after the interaction, western blot - with immunostaining using convalescent patient serum - revealed two reactive bands at ~70 kDa and ~55 kDa in the total extract, one at ~70 kDa in the unbound fraction, and two bands (one intensely reactive at ~55 kDa and the other at ~45 kDa) in the bound fraction (**Fig. 3c**).

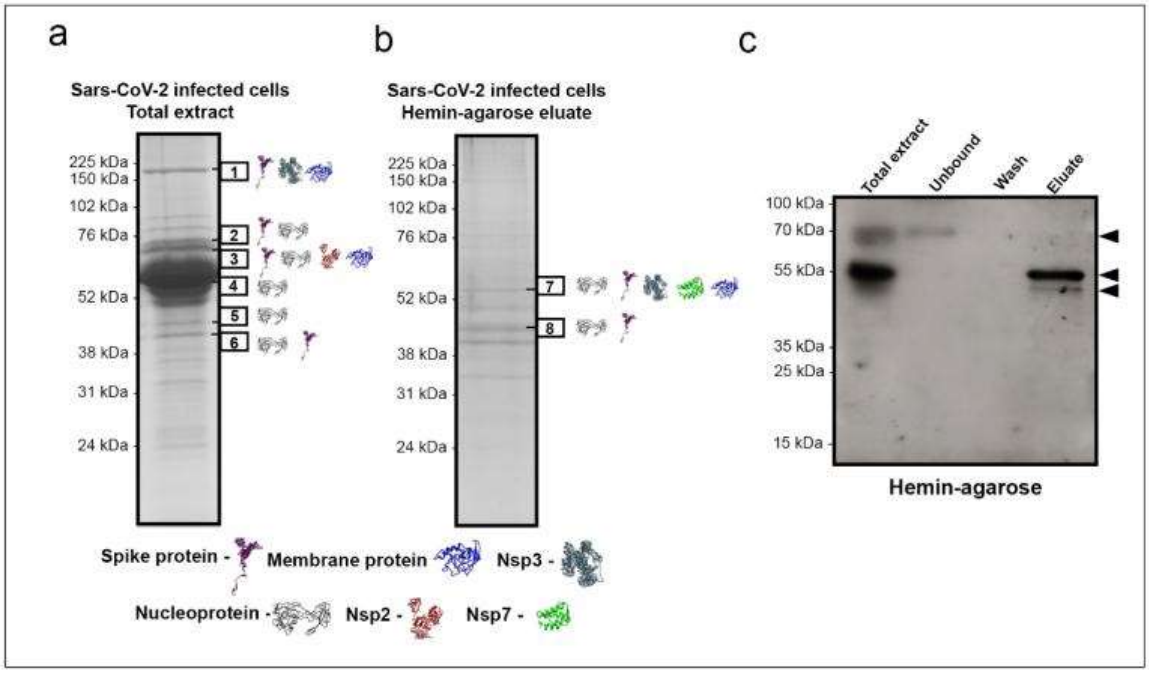

Fig. 3: Heme affinity purification of proteins from total extracts of SARS-CoV-2 infected Vero cells and their identification by mass spectrometry. SDS-PAGE separated proteins stained by Coomassie blue from (a) whole protein extract of virus-infected Vero cells and (**b**) eluate from a hemin-agarose purification. Bands excised for protein identification by LC-MS/MS are indicated by black boxes 1-8. The proteins identified were nucleoprotein (P0DTC9), membrane protein (P0DTC5), Spike protein (P0DTC2), and Replicase polyprotein 1a/1ab (P0DTC1/P0DTD1). The peptides in the replicase polyprotein 1a/1ab were identified as Nsp2, Nsp3, and Nsp7. The identified proteins in each band are shown as 3D structures retrieved from the I-Tasser site (https://zhanglab.ccmb.med.umich.edu/I-TASSER/). (**c**) Western blot with immunostaining - using COVID-19 patient convalescence serum to detect reactivity - from hemin-agarose chromatography fractions of protein lysate from SARS-CoV-2-infected Vero cells; arrowheads indicate two bands revealed in the eluate.

The observation that viral proteins can bind to hemin suggested that this interaction could extend to Hb. To test this hypothesis, an overlay assay was performed with Hb on SARS-CoV-2 infected Vero cell extracts separated by SDS-PAGE and transferred to a nitrocellulose membrane (**Fig. 4a)**. Haptoglobin, used as a positive control, displayed the predicted size for the β-chain at 40 kDa and showed that this approach could detect Hb binding proteins; it revealed two protein bands (~150 kDa and ~75 kDa) exclusively in SARS-CoV-2-infected cells, while the other bands (~95 kDa, ~70 kDa, and ~50 kDa) were also found in the mock cell extract. Based on the results from mass spectrometry, the bands' sizes suggested the Spike protein presence (Fig. 4a). To confirm this conclusion and refine the region in Spike glycoprotein that could interact with Hb, a protein-protein interaction assay was performed using the Spot Synthesis technique. An array of 15-mer peptides with a 5 amino acid overlap representing the RBD region of the Spike protein synthesized *in situ* on a cellulose membrane was constructed. Following Hb's incubation and its subsequent detection by Hb-specific antibodies with corresponding secondary

antibodies, several highly reactive spots were revealed that indicated the natural motifs interaction between sequences in the RBD and Hb (**Fig. 4b, top panel**). The relative intensity percentage was calculated, and individual peptide sequences were identified; signal intensities above 50% were considered the cutoff for a positive reaction. Five unique peptide sequences were defined that interacted with Hb (**Fig. 4b, lower panel**). Molecular docking assay of protein/protein interactions indicated the possibility of binding the spike protein with the alpha and beta hemoglobin domains (**Fig. 4c**), showing binding energy of -460 kcal/mol (**Supplementary Figure 3**). The data showed that this binding could be coordinated by four hot spot amino acid residues (**Supplementary Table 2**) from both proteins: Spike (Tyr341, Tyr351, Phe347, Arg346, Tyr451, and Leu452) and Hb (His46, His51, Gln55, and Asp48) (**Fig. 4d**).

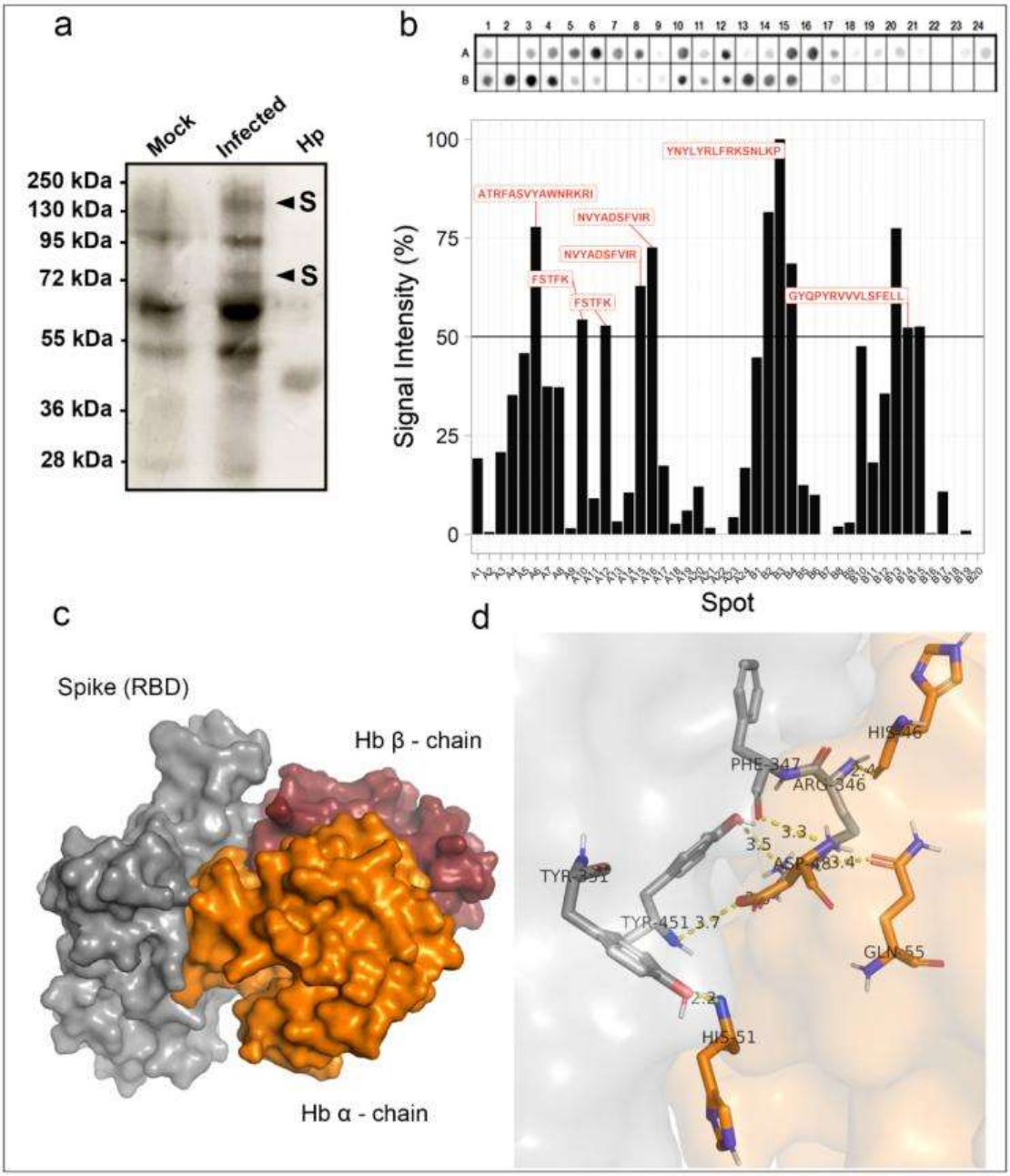

Fig. 4: Hemoglobin (Hb) binding to Spike protein and its RBD. (**a**) Total protein extracts (20 μg) of SARS-CoV-2-infected Vero E6 cells (Infected) or mock-infected cells (Mock; 20 μg) were separated by SDS-PAGE (10%) along with haptoglobin (Hp; 2 μg), transferred to a nitrocellulose membrane, and serially incubated with Hb (10 μg/mL), anti-Hb antibody, and peroxidase-conjugated secondary antibodies. After substrate, two 72 and 150 kDa bands were exclusively found in SARS-CoV-2 infected extract (arrowheads). (**b**) Spot synthesis analysis with a library of 15-mer peptides offset by five amino acids to represent the RBD region of the Spike protein synthesized directly onto a cellulose membrane followed by probing with Hb (5 μg/mL) and revealed by anti-human Hb antibodies. The top panel shows the chemiluminescent image of signals from peptides bound to Hb. The bottom panel shows a graph of the signal intensities normalized to the maximum signal. An intensity level above 50% defined Hb-reactive peptides. Molecular docking of SARS CoV-2 spike protein with human hemoglobin (n=1). (**c**) Interaction of spike protein (gray) with α-chain Hb (orange) and β-chain (red). (**d**) Representation of amino acid residues binding to spike protein (sticks and gray) with α-chain of hemoglobin (orange). Source data are provided as a Source Data file.

Hemin, hemoglobin, and PpIX affect SARS-CoV-2 adsorption and replication.

The intense interaction between peptides in the RBD of the Spike and localization of Hb in the molecular model suggested that the presence of free Hb could competitively interfere with the binding of SARS-CoV-2 to ACE2, its receptor on host cells. As such, we hypothesized that the addition of Hb could impair virus replication in an *in vitro* assay. To test this hypothesis, Vero cells were pretreated with a sub-optimal Hb concentration (1 μM) for 1 h at 37 °C before their exposure to the virus and then infected SARS-CoV-2 at MOI of 0.01. Alternatively, the virus was preincubated with 1 μM of Hb for 1 h before its addition to Vero cells for another hour at 37 °C. After 24 h, culture supernatants were collected, and the production of infectious virus particles was quantified by plaque assay. The pretreatment of Vero cells with Hb did not affect virus production (**Fig. 5a, left column**); however, the virus's preincubation with Hb reduced approximately 52.0 ± 1.3 % of virus replication. Convalescent plasma was used as a positive control for viral neutralization and inhibited viral replication (100 %)(**Fig. 5b, left column**). Hemin and PpIX were also tested to evaluate if porphyrin-protein interactions could affect virus replication. Hemin displayed no or little effect in virus replication when used as a pretreatment of Vero cells or SARS-CoV-2, respectively (**Fig. 5a and 5b, center columns**). PpIX inhibited SARS-CoV-2 replication by 90.0 ± 1.8 and 100 % when used as a pretreatment of the cells or virus, respectively (**Fig. 5a and b, right columns**).

Next, we analyzed if viral replication reduction was related to Hb binding interference with a receptor-mediated virus attachment. An adsorption inhibition assay was performed. The incubation of the virus with cells was performed at 4 °C for 1 h to minimize internalization, and then viral RNA was purified for quantification by RT-PCR. When SARS-CoV-2 was pre-incubated with Hb (1 μM) for 1 h at 37 °C and then applied to Vero cells at an MOI of 0.01, a reduction of 58.1 ± 29.6 % was measured in the virus adsorption (**Fig. 5c**). Hemin (1 μM) reduced virus attachment by approximately 40 %, and PpIX reduced virus attachment by 61.3 ± 18.0 %. When cells were treated with 1 μM of either Hb, hemin, or PpIX, after

the initiation of infection by SARS-CoV-2, virus replication was inhibited 99.5 ± 0.4 % by Hb, 100 % by PpIX, and 29.1 ± 7.2 % by hemin **(Fig. 5d**).

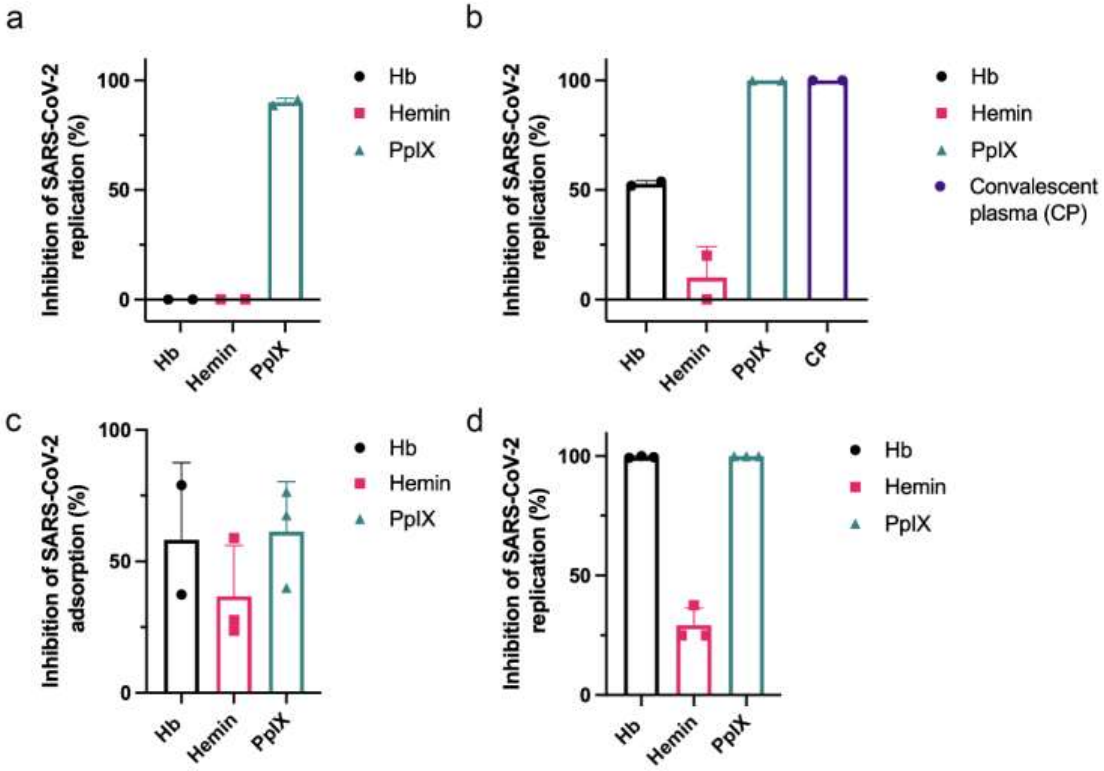

Fig. 5: Inhibition of SARS-CoV-2 replication and attachment by porphyrins and Hb. (**a-b**) Vero E6 cells (**a**) or SARS-CoV-2 (**b**) were pre-incubated with 1 µM of Hb, hemin, or PpIX for 1 h at 37 °C before the start of infection with an MOI of 0.01 for an additional hour at 37 °C. Culture supernatants were collected after 24 h, and the virus titer was determined by plaque assay (n=2). A convalescent plasma of an infected patient (1:3 dilution) was used as the positive control. (**c**) SARS-CoV-2 was incubated at 1 µM Hb, hemin, or PpIX for 1 h at 37 °C before introducing Vero E6 cells at an MOI of 0.01 for 1 h at 4 °C. Rinsed cell monolayers were lysed, and RT-PCR quantified the virus content. Cumulative data (Hb: n=2, Hemin: n=3, PpIX: n=3). (**d**) Vero E6 was infected with SARS-CoV-2 at an MOI of 0.01 for 1 h at 37 °C and then treated with 1 mM of hemin, PpIX, or Hb. After 24 h, supernatants were collected, and the virus titer was quantified by PFU/mL (Hb, Hemin, PpIX: n=3). Data represented the percentage of inhibition compared to control (infected and untreated) and expressed as mean with standard deviation. Source data are provided as a Source Data file.

Discussion

Severe COVID-19, caused by SARS-CoV-2, typically leads to pneumonia and acute respiratory distress syndrome (ARDS). However, the growing list of evidence indicates a systemic impairment that leads to multiorgan failure. During an infection, an imbalance in the immunological response can produce a "cytokine storm" and numerous other pathophysiological processes such as hypoxemia, thrombosis, pulmonary embolism, encephalopathy, myocardial injury, heart failure, and acute kidney injury20. Hematological dysfunction in severe COVID-19 includes low levels of erythrocytes and an increased variation in the red blood cell

distribution width (RDW)8,9. Recent reports on the immune effects of COVID-19 have highlighted immune thrombocytopenia and autoimmune hemolytic anemia21. Other evidence suggests an increase in hemophagocytosis that could be related to elevated levels of ferritin in COVID-1922. In hemolytic disorders, the release of high amounts of Hb and heme trigger proinflammatory response, complement activation, and procoagulant and pro-oxidative environment [23,24].

Recently, an *in silico* analysis hypothesized that viral proteins could bind Hb beta-chains that would be expected to interfere with O2 transport and heme metabolism6. Another finding suggested that the sequence similarity between SARS-CoV-2 Spike protein and hepcidin, a peptide hormone involved in iron metabolism, could lead to an imbalance of iron metabolism7. Yet, in the absence of experimental data, it is not clear if SARS-CoV-2 proteins actually can interact with Hb and displace iron from heme.

To decipher these possible interactions, *in silico* analysis was performed to identify heme-binding motifs in viral proteins. Commonly, heme coordination can occur by hydrogen bonds via propionate groups, π-π stacking, electrostatic and hydrophobic interactions. The critical heme-coordinating amino acids are histidine, cysteine, and tyrosine; methionine and lysine occur at a lower frequency [25,26]. Here, *in silico* analysis supported the potential interaction of porphyrin ring with Tyr333 of the N protein in addition to hydrophobic and hydrogen bonds via propionate side chains. An open question is whether heme is a necessary endogenous cofactor recruited by viral proteins during replication and translation. The primary function of the N protein is to bind RNA. This protein comprises an N-terminal domain containing the RNA-binding site, a C-terminal dimerization domain, and a central linker region rich in serine and arginine [27]. The heme-binding motifs identified in the N protein suggest another function for this protein. The analyses of other N protein motifs identified a nuclear localization signal and a nuclear export signal that offer dynamic nuclear-cytoplasmic trafficking that can be involved in transcription regulation [27].

N protein binding to heme might have an important implication in viral and cellular transcriptional regulation since heme regulates multiple transcription factors in the nucleus, modulating the expression of various genes [28]. Interestingly, high-confidence protein-protein interactions between SARS-CoV-2 and human proteins identified N protein associated mainly with components of cellular translational machinery [29]. N protein was reported to interact with two subunits of casein kinase 2 (CK2), a protein involved in activation of heme regulator inhibitor (HRI) kinase that phosphorylates eukaryotic initiation factor 2 (eIF-2), inhibiting translation [30]. N protein could be involved in dissociation or recycling of heme from HRI, modulating the phosphorylation of eIF2-α [31]. Some viruses do not require eIF-2 and even induce host translation shutdown [32]; possibly, these events consist of a manipulation route for viral protein synthesis.

Electrophoresis of mock and SARS-CoV-2 infected cells revealed different heme-binding profiles. The electrophoretic mobility in the TMB in-gel staining assay

suggests that Spike fragment (S1 and S2, ~70kDa) and nucleoprotein (55 kDa) could bind hemin and retained its peroxidase activity. Also, heme-binding interactions in solution were changed by viral infection. Due to their hydrophobicity, heme and PpIX have low solubility in an aqueous solution and tend to aggregate. Binding complex with proteins can cause redshift and increase the Soret band's intensity, and change spectra profile of Q band [33]. However, these results could also indicate a viral modulation of cellular hemeproteins or heme-binding proteins.

To refine the analysis, shotgun proteomics was performed to identify SARS-CoV-2 heme-binding proteins. Identification of proteins in SARS-CoV-2-infected Vero cells total extract revealed structural and non-structural proteins. Spike holoprotein was placed in the expected gel migration range (Band 1), but also cleavage products S1 and S2 produced by proteases (TMPRSS2, furin, cathepsin) were observed at ~70 kDa bands (Band 2 and 3). Interestingly, SARS-CoV's mass spectrometry analysis also identified Spike protein in bands of relative molecular masses divergent from their theoretical sizes, suggesting glycosylation and cleavage [34]. As expected, nucleoprotein was frequently identified and found in bands at 55 kDa, 45 kDa, and 40 kDa. The 55 kDa band in the TMB in-gel staining assay firmly retained hemin. The N protein presence in bands with different predicted molecular masses has been previously noted in SARS-CoV but attributed to protein degradation [35].

Interestingly, N protein was identified in a 46 kDa band of nucleus fraction of infected cells [35]. The transition to a higher molecular mass has been observed for nucleoprotein protein using mass spectrometry [34]. It can be indicative of the complexity of protein-protein binding dynamics in the replication of SARS-CoV-2. Since albumin in culture medium masks low abundance proteins identification [36], we performed a serum depletion followed by affinity chromatography using hemin-agarose beads. This approach increased the overall identification of proteins, and after purification, the N protein was the most abundant protein identified by mass spectrometry in the 45 kDa band. A variety of protein-protein interactions are essential for SARS-CoV-2 replication and viral assembly, such as its structural proteins that have been reported to interact with each other [37]. In the hemin-agarose eluate, the M protein was identified in band 7 at a higher relative molecular mass position than its predicted molecular mass of 25 kDa. It is a transmembrane glycoprotein that comigrated with the other structural proteins Spike and N. While the interaction of the M protein with the N protein has been observed previously and appears to be necessary to viral assembly [38], this comigration was not observed in the total extract of proteins from virally infected Vero cells before the inclusion of the heme-agarose beads. N and S protein are highly immunogenic, unlike M protein [39]. Spike protein appears to bind weakly to hemin beads since no 70 kDa immunoreactive bands were noticed in the eluate fraction.

The heme-binding capacity of viral proteins leads us to question if this could extend to Hb. In the overlay assay, the bands of approximately 150 kDa and 70 kDa, which were exclusively found in the virus-infected cell extract, matched the Spike holoprotein's predicted size and fragments S1 and S2. The identification of Spike as

a significant viral protein in these bands opens Hb's question and could bind and interact with the RBD region. The Spot-synthesis analysis demonstrated several areas of the RBD of the Spike protein bind Hb, corroborating the molecular docking analysis. The apparent strength of binding according to the strong signals and Hb's positioning on the Spike protein suggests that its interaction with Spike could hinder viral entry and subsequent replication. In fact, the highest spot signal (448YNYLYRLFRKSNLKP463) was observed within the receptor-binding motif region (RBM; 437-508). This region is responsible for binding to ACE2 and includes hot spot residues that bind Hb (Tyr451 and Leu452). It is essential to highlight that, so far, the most frequent mutations in the RBD region of new variants are located in RBM (Tyr453, Gly476, Phe486, Thr500, and Asn501) but are not present in hot spot amino acids that interact with Hb [40].

Additionally, binding of Spike with hemoglobin may have a role in COVID-19 pathophysiology. Meta-analysis revealed that severe COVID-19 patients had decreased hemoglobin levels, lower RBC count, and higher RDW than moderate COVID-19 cases [41]. Although a combination of events plays a role in COVID-19 hypoxemia [42], the decrease in Hb levels contributes to hypoxia and is related to complications, ultimately leading to multiorgan failure41. Low hemoglobin levels were attributed to hemolytic anemia driven by inflammation and iron dysmetabolism, interfering with erythropoiesis [21,41]; our results demonstrated that viral particles' binding could also be implicated. In the scenario of hemolytic anemia, an excess of heme/Hb increases ROS levels and tissue damage leading to vascular injury and ferritin overexpression [43]. High ferritin levels are a hallmark of COVID-19, eventually contributing directly to inflammation and lung injury since ferritin is proinflammatory and leads to ferroptosis [7,44]. A recent report found that even after two months from the onset of disease, 30% of patients still presented iron deficiency, hyperferritinemia (38%), and anemia (9.2%) correlated with disease severity [44].

Additionally, free heme and hemoglobin are involved in hemostasis and thrombosis. Hb enhances platelet activation by scavaging nitric oxide23 and also induces platelet aggregation contributing to prothrombotic events [45]. The assembly of viral particles and hemoglobin capping of Spike could contribute to COVID-19 thromboembolic events and aggravate lung injury in critically ill patients. Hemolysis in the intravascular and alveolar spaces results in hemoglobin release that can contribute to organ disfunction [46]; in ARDS, it is proposed that hemoglobin-mediated damage by cell surface receptor binding on the alveolar epithelium is independent of oxidative stress [47].

The ability of porphyrins to interfere in receptor binding was observed through *in vitro* assays. Hemin alone had little effect on viral attachment and replication, suggesting that hemin has little to no direct interactions with the Spike protein or ACE-2. As intracellular concentrations of hemin are highly regulated, and hemin can be exported or degraded by heme-oxygenase11, the absence of an effect is consistent with its physiology. In contrast, exposure of either cell or virus to PpIX

dramatically reduced viral load. Similar outcomes for PpIX and verteporfin have been recognized against SARS-CoV-2 since treatment with porphyrins interferes with the ACE2 and Spike that would impair viral entry. Also, these drugs were able to inhibit viral RNA production, suggesting other potential mechanisms of action19. Likewise, our results showed that PpIX at 1μM could inhibit viral replication after 24 h19. PpIX is hydrophobic and could interact with membranes; thus, porphyrin interaction with viral envelope can induce destabilization and oxidation [48].

Pretreatment of viral particles with Hb reduced approximately 50% of both viral replication and adsorption, demonstrating Spike/RBD-ACE-2 fusion impairment. Furthermore, Hb treatment's effect after viral infection was higher, reducing 99% of viral replication. Modulation of viral replication by extracellular free Hb can occur via prooxidant activity, direct interactions of globin or heme to cell components and signaling pathways, and induction of heme oxygenase [49]. Down-regulating HO-1 is a strategy for the optimization of virus replication and to evade host antiviral mechanisms for hepatitis C virus (HCV), hepatitis B virus (HBV), and Pseudorabies virus (PRV) infection [50–52]. HO-1 is a critical stress-induced enzyme that promotes antioxidant, antiapoptotic, and anti-inflammatory activities via downstream metabolites such as biliverdin and bilirubin [53]. Biliverdin impairs HCV replication by inducing an interferon response [52]. Induction or overexpression of HO-1 inhibits some virus-like influenza [54], HIV [55], human respiratory syncytial virus (RSV) [56], and Zika [57].

Overall, our demonstration that SARS-CoV-2 proteins can bind to heme or Hb may have clinical implications. Mainly, Hb's interaction with Spike opens new therapeutic perspectives due to significant virus attachment and replication inhibition. Also, this binding could potentially increase or drive hematological disorders and thrombosis observed in severe COVID-19. There are still knowledge gaps on viral-host cell complex interplay and disease pathophysiology, the data presented here will contribute to scientific discussion. More research will be needed to confirm the relevant implications of these heme-protein interactions and correlations with COVID-19 physiopathology.

Material and methods

Motifs identification

The MEME Suite server identified the motifs for binding to the heme group on the SARS-CoV-2 nucleoprotein [58]. Protein sequences from 68 crystallized structures with a heme group. Then, 36 Hb sequences deposited in the Uniprot database (www.uniprot.org) were used against 13 nucleoprotein sequences from SARS-CoV-2.

Molecular docking

Receptor-Ligand: Molecular docking assays were employed to predict the binding modes of the Sars-CoV-2 nucleoproteins (PDB code - 6zco; accessed day September

08, 2020 - https://www.rcsb.org/) and ligand heme prosthetic group (Fe-protoporphyrin) complexes by using the DockThor server (https://dockthor.lncc.br /v2/). Structures with positional root mean square deviation (RMSD) ≤ 2 Å were clustered, and results with the most favorable free energy of binding were selected.

Protein-Protein: This assay was performed with human hemoglobin (PDB code -4x0i) and spike protein (PDB code -7kn5), both accessed day September 20, 2020, by using RosettaDock server (http://rosettadock.graylab.jhu.edu). The alpha and beta chains of hemoglobin were assessed in the protein interaction assays and evaluated using the HOTREGION database (http://prism.ccbb.ku.edu.tr/hotregion/_index.php).

Cell culture, virus expansion, and virus tittering

African green monkey kidney (Vero, subtype E6, ATCC®CRL-1586™) cells were cultured in media consisting of high glucose DMEM complemented with 10% fetal bovine serum (FBS; HyClone, Logan, Utah), 100 U/mL penicillin, and 100 µg/mL streptomycin (Pen/Strep; Thermo Fisher Scientific). Cells were maintained in a humidified atmosphere with 5% CO_2 at 37 °C. The SARS-CoV-2 used in these studies (GenBank #MT710714) was isolated from a nasopharyngeal swab obtained from a consenting patient with COVID-19, as confirmed by RT-PCR. The virus was expanded in Vero E6 cells at a multiplicity of infection (MOI) of 0.01 according to WHO guidelines that mandate all procedures related to virus cultures be performed in a biosafety level 3 (BSL3) facility.

Virus titer was defined as plaque-forming units (PFU)/mL. Briefly, Vero E6 cells were seeded into 96-well plates at 2 x 10^4 cells/well for 24 h before exposure to a serial dilution of expanded SARS-CoV-2 for 1 h at 37 °C. A semi-solid high glucose DMEM medium containing 2 % FSB and 2.4 % carboxymethylcellulose was added, and cultures were incubated for 3 days at 37 °C. Then, the cells were fixed with 10 % formalin for 2 h at room temperature. The cell monolayer was stained with 0.04 % solution of crystal violet in 2 0% ethanol for 1h. Virus stocks were stored at -80 °C until use.

Yield reduction assays and virus titration

Vero cells were seeded into 96-well plates at a density of 2 x 10^4 cells/well for 24 h at 37 °C before exposure to SARS-CoV-2 at an MOI of 0.01. After a 1 h incubation, the inoculum was removed, and cells were incubated in a medium containing 1 µM of the experimental compounds diluted in DMEM with 2 % FBS. Alternatively, two experimental conditions were performed: i) preincubation of the virus with the compounds (1 µM) for 1 h at 37 °C before their addition to Vero E6 cells (MOI of 0.01) for an additional hour, or ii) preincubation of Vero cells with the compounds (1 µM) for 1 h at 37 °C before their exposure to the virus (MOI 0.01). After 24 h, supernatants were collected for virus titration (PFU/mL) as described above. For virus titration, Vero E6 in 96-well plates (2 x 10^4 cells/well) were infected with serial dilutions of yield reduction assays' supernatants containing SARS-CoV-2 for 1 h at

37 °C. A semi-solid high glucose DMEM medium containing 2 % FSB and 2.4 % carboxymethylcellulose was added, and cultures were incubated for 3 days at 37 °C. Then, the cells were fixed with 10% formalin for 2 h at room temperature. The cell monolayer was stained with 0.04 % solution of crystal violet in 20% ethanol for 1 h. The virus titers were determined by plaque-forming units (PFU) per milliliter.

Adsorption inhibition assays

The virus was incubated with compound (1 μM) for 1 h and then added to monolayers of Vero E6 cells in 48-well plates (5 x 105 cells/well) at an MOI of 0.01 for 1 h at 4 °C. The medium with the virus was removed, and cells washed three times with medium before lysis buffer addition. Total viral RNA was extracted using QIAamp Viral RNA (Qiagen®) according to the manufacturer's instructions. Quantitative RT-PCR was performed using GoTaq® Probe qPCR and RT-qPCR Systems (Promega) in a StepOne™ Real-Time PCR System (Thermo Fisher). Amplifications were performed as 25 μL reactions containing 1x reaction mix buffer, 50 μM of each primer, 10 μM of the probe, and 5 μL of RNA template. Primers, probes, and cycling conditions followed the recommendations of the Centers for Disease Control and Prevention (CDC) protocol for the detection of the SARS-CoV-2 [59]. A standard curve was included for virus quantification [60].

SDS-PAGE and hemin-binding blots

Vero E6 cells were infected with SARS-CoV-2 at a multiplicity of infection (MOI) 0.01 for 1 h at 37 °C. The inoculum was removed, and a fresh culture medium was added. Protein extracts (20 μg) were obtained 24 h post-infection by lysing the cell monolayer with lysis buffer (100 mM Tris-HCl pH 8.0, 150 mM NaCl, 10 % glycerol, 0.6 % Triton X100). Protein extracts were electrophoretically separated on a 10 % SDS-PAGE using Laemmli`s buffer [61]. For hemin-binding blots, proteins were transferred to nitrocellulose membrane and then rinsed with Tris-buffered saline [TBS (10 mM Tris-HCl pH 8.0 containing 150 mM NaCl)] plus 0.1% Tween 20 (TBST) followed by 1 h incubation with TBS containing hemin (2 μM). Membranes were subsequently washed three times for 30 min with TBST and revealed with a solution containing 0.1 mg/mL 3,3' diaminobenzidine (DAB), 0.1 % H2O2, 10 mM HEPES, pH 6.2, and 100 μM CaCl2 overnight at 4 °C in the dark [62]. Alternatively, heme-binding proteins were evaluated by 1 h room temperature incubation of the protein extracts (20 μg) with hemin (300 μM) in 250 mM Tris-HCl, pH 8.0, 5 mM EDTA, and 10% glycerol, followed by SDS-PAGE [63]. Then, gels were washed for 1 h with PBS containing Triton X-100 (2.5 %) and equilibrated for 30 min with sodium acetate 0.5 M (pH 5.0). Heme binding proteins were revealed with 2 mg/mL 3,3',5,5'-tetramethylbenzidine (TMB) dissolved in 15 mL of methanol and 35 mL of 0.5 M sodium acetate (pH 5.0). Then, 300 μL of 30 % H2O2 solution was added, and the reaction was carried out for 30 min in the dark. After a blue-colored band developing, indicative of a heme-protein complex, the gels were washed with

598 sodium acetate (pH 5.0) and isopropanol (30 %) solution. Protein extract without
599 preincubation with hemin was used as a negative control.
600
601 **Hemin and PPIX binding assay**
602 Hemin chloride (10 μM) diluted in NaOH (0.1 M) was added to a quartz cuvette
603 containing 20 μg of protein extract from Vero cells and SARS-CoV-2 infected Vero
604 cells. The absorbance of samples was evaluated at 300–700 nm. Spectroscopic
605 analysis was performed using a SpectraMaxM2e (Molecular Devices). For
606 protoporphyrin IX (PPIX) binding assays, 20 μg of each protein extract was
607 incubated with PPIX solution (1mM in DMSO followed by dilution to 1 μM in
608 phosphate buffer saline pH 7.4) followed by absorbance spectra analysis.
609
610 **Protein purification and hemin-agarose binding assay**
611 Protein extract, obtained from infected Vero E6 monolayers 24 h post-infection lysed
612 with 100 mM Tris-HCl pH 8.0, 150 mM NaCl, 10 % glycerol, 0.6 % Triton X-100, was
613 initially subjected to affinity chromatography using a protein-A/anti-BSA mAB
614 matrix (Sigma-Aldrich) to remove excess albumin (a heme-binding protein
615 contaminant). Then, hemin-agarose was used to isolate heme-binding proteins.
616 Briefly, 200 mL of hemin-agarose (Sigma-Aldrich) was washed three times in 1 mL
617 of 100 mM NaCl, 25 mM Tris-HCl (pH 7.4) 5 min, and centrifugated at 700 *g*. Next,
618 hemin-agarose was incubated for 1 h at 37 °C, under agitation, with SARS-CoV-2
619 protein extracts (800 μg). The unbound proteins were removed by washing three
620 times with equilibration buffer, and beads incubated for 2 min with elution solution
621 (2 %, SDS, 1 % β-mercaptoethanol in 500 mM Tris HCl, pH 6.8) followed by boiling
622 at 100 °C for 5 min [64]. Total extract, unbound (supernatant) fraction, washing
623 fraction, and hemin-agarose bound proteins were separated by 10 % SDS–PAGE
624 gels and stained with Coomassie Blue R-250 or transferred to a nitrocellulose
625 membrane (subsequently blocked with TBS-T (Tris-buffer saline, 0.1% Tween 20,
626 pH 7.5) and 5% defatted milk. Immunostaining was later performed by incubating
627 membranes overnight at 4 °C with a pool of COVID-19 convalescent serum (1:200).
628 Then, membranes were washed and incubated with HRP-conjugated anti-human
629 IgG antibody (Sigma-Aldrich; 1:10.000) followed by chemiluminescence detection.
630
631 **Overlay assay**
632 Protein extracts (20 μg), obtained as described above, were separated by 10 % SDS–
633 PAGE and transferred to a nitrocellulose membrane (Bio-Rad). Haptoglobin
634 (Sigma-Aldrich) was used as a control. The membrane was blocked with 2 % BSA
635 in TBS-T buffer, then incubated overnight at 4 °C after adding 10 μg/mL of human
636 hemoglobin (Hb). After washing with TBS-T, the membrane was incubated with an
637 anti-Hb antibody (1:5.000) (Sigma-Aldrich). The antigen-antibody complex was
638 revealed by chemiluminescence.
639
640 **Spot-Synthesis**

The DNA sequence of the Spike protein (P0DTC2) receptor-binding domain was retrieved from Uniprot. A library of 15 amino acid peptides with a 5-amino acid overlap was designed to represent the entire coding region (319-541 aa) of RBD and automatically synthesized onto cellulose membranes using an Auto-Spot Robot ASP222 (Intavis, Koeln, Germany) according to the SPOT synthesis protocol [65,66]. Briefly, membranes containing the synthetic peptides were washed with TBST (and then blocked with TBS-T containing 1.5 % BSA under agitation for 2 h at room temperature. After extensive washing with TBS-T (Tris-buffer saline, 0.1 % Tween 20, pH 7.0), membranes were incubated overnight with Hb (5 μg/mL) dissolved in TBST + BSA (0.75 %). After incubation, membranes were washed with TBS-T, followed by additional incubation with anti-human Hb antibody for 90 min. Subsequently, the membrane was washed with TBS-T and incubated for 90 min with anti-rabbit IgG antibody conjugated to alkaline phosphatase (Sigma Alrich), diluted 1:5.000 in TBS-T solution containing 0.75 % BSA. Washes were performed with TBS-T followed by the addition of substrate for chemiluminescent alkaline phosphatase Tropix® was added. Next, membranes were washed three times with TBS-T, and then the buffer was exchanged to CBS (50 mM citrate-buffer saline) before the addition of the chemiluminescent enhancer Nitro-Block II. The chemiluminescent substrate Super Signal R West Pico was applied, and signals were immediately detected. A digital image file was generated, and the signal intensities quantified using TotalLab (Nonlinear Dynamics, USA) software[66]. The spots with signal intensity greater than or equal to 50% of the highest signal value obtained in all membrane spots were considered to identify possible binding motifs.

In-Gel Trypsin Digestion of Proteins.

Protein spots were excised from gels using sterile stainless steel scalpels, transferred to 0.5 mL tubes, and cut into smaller pieces. In-gel digestion with trypsin (Promega V511A) was performed according to the literature [67] with modifications described elsewhere [68]. Protein reduction was performed by the addition of 100 μL of 65 mM DTT for 30 min at room temperature, followed by alkylation with 100 μL of a 200 mM iodoacetamide solution for 30 min, in the dark, at room temperature. After washes and trypsinization, the final 80 μL peptide-containing samples were concentrated by vacuum centrifugation to approximately 20 μL and stored at −20 °C until mass spectrometric analysis. Gel pieces from a "blank" region and the BSA molecular mass marker were negative and positive controls, respectively.

Identification of proteins by mass spectrometry

The tryptic digests were analyzed in three technical replicates by reversed-phase nanochromatography coupled to high-resolution nanoelectrospray ionization mass spectrometry. Chromatography was performed using a Dionex Ultimate 3000 RSLCnano system coupled to the HF-X Orbitrap mass spectrometer (Thermo Fischer Scientific). Samples (4 μL per run) were initially applied to a 2 cm guard column, followed by fractionation on a 25.5 cm PicoFritTM Self-Pack column (New

Objective) packed with 1.9 µm silica, ReproSil-Pur 120 Å C18-AQ (Dr.Maisch/ Germany). Samples were loaded in 0.1 % (v/v) formic acid (FA) and 2 % acetonitrile (ACN) onto the trap column at 2 µL/min, while chromatographic separation occurred at 200 nL/min. Mobile phase A consisted of 0.1% (v/v) FA in water, while mobile phase B consisted of 0.1% (v/v) FA in ACN. Peptides were eluted with a linear gradient from 2 to 40% eluent B over 32 min, followed by up to 80% B in 4 min. Lens voltage was set to 60 V. Full scan MS mode was acquired with a resolution of 60,000 (FWHM for *m/z* 200 and AGC set to $3x10^6$). Up to 20 most abundant precursor ions from each scan (*m/z* 350-1,400) were sequentially subjected to fragmentation by HCD. Fragment ions were analyzed at a resolution of 15,000 using an AGC set to $1x10^5$. Data were acquired using Xcalibur software (version 3.0.63).

Peptide identification and protein inference

All MS/MS spectra were analyzed using PEAKS Studio X Plus (Bioinformatics Solutions, Canada). Peptide identification was performed against *Chlorocebus sabaeus* reference proteome at the UNIPROT database under ID UP000029965, plus the SARS-CoV-2 reference proteome at the same database UP000464024 (downloaded July 03, 2020). Data refinement applied the precursor correction (mass only). Next, PEAKS *de novo* analysis was run assuming trypsin digestion, with a fragment ion mass tolerance of 0.02 Da and a parent ion tolerance of 10 ppm. Cysteine carbamidomethylation (+57.02 Da) was set as fixed modification; a maximum of 2 variable shifts per peptide was allowed. PEAKS DB analysis was performed using these same parameters, plus the possibility of up to two missed enzyme cleavages and nonspecific cleavage at both sides of the peptides. Finally, post-translational and other possible modifications were searched using the PEAKS PTM algorithm, with the same parameters described above, against a protein subdatabase composed only by protein entries found by the previous PEAKS De Novo and PEAKS DB searches. False discovery rates (FDR) were estimated through the PEAKS decoy fusion approach. A peptide-spectrum match FDR of 0.1 % and protein identifications with at least 2 unique peptides were the criteria used to establish FDR values at peptide and protein levels smaller than 1 %.

Data analysis

Graphs were prepared, and statistics were performed using R software 4.0.0 and GraphPad Prism version 9.

Conflict of interest

The authors declare no conflict of interest.

Author Contributions

GCL, FSS, SGS, and TMLS conceived and designed the proposal. GCL, MCSP, RHV, TMLS, SGS, and DWP wrote the paper. GCL, FSS, CQS, SSGD, NFR, JRT, and PNP performed *in vitro* experiments and processed the data. FSS, CRA, and NC performed *in silico* and docking analysis. MROT and RHV performed mass

spectrometry and data analysis. Contributed with reagents/materials/analysis: SGS, TMLS, MCSP, MROT, and RHV. All authors have read and agreed to the published version of the manuscript.

Funnding

SGS received support from FIOCRUZ (INOVA VPPCB-007FIO-18-2-21 and VPPIS-005FIO-20-2-51), Carlos Chagas Filho Foundation for Research Support of the State of Rio de Janeiro/FAPERJ #(grant E-26 110.198-13), and the Brazilian Council for Scientific Research/CNPq #(grant 467.488.2014-2 and #301744/2019-0).
DWP received support from FIOCRUZ (INOVA VPPCB-005-FIO-20).)
TMLS received support from FIOCRUZ (INOVA B3-Bovespa)

Acknowledgments

SGS, CRA, MCSP and RHV are Post Doctorate fellows from CNPq.
GCL is Post Doctorate fellow from CINCT-IDPN/FAPERJ (E-26/201.848/2020)
FSS is Post Doctorate fellows from CAPES.
CQS, NFR and JTR are postdoctoral fellows from CAPES/CDTS and Inova Program.
SSGD is a PhD student from Oswaldo Cruz Institute/Fiocruz.

References

1. Li Q, Guan X, Wu P, Wang X, Zhou L, Tong Y, et al. Early transmission dynamics in Wuhan, China, of novel coronavirus–infected pneumonia. N Engl J Med 2020; 382: 1199-07.
2. To KK, Tsang OT, Leung WS, Tam AR, Wu TC, Lung DC, et al. Temporal profiles of viral load in posterior oropharyngeal saliva samples and serum antibody responses during infection by SARS-CoV-2: an observational cohort study. Lancet Infect Dis 2020; 20: 565-74.
3. Kannan S, Shaik Syed Ali P, Sheeza A, Hemalatha K COVID-19 (Novel Coronavirus 2019) - recent trends. Eur Rev Med Pharmacol Sci 2020; 24: 2006-11.
4. Ho D, Wang P, Liu L, Iketani S, Luo Y, Guo Y, et al. Increased resistance of SARS-CoV-2 variants B.1.351 and B.1.1.7 to antibody neutralization. Res Sq 2021; rs.3.rs-155394.
5. WHO Solidarity Trial Consortium, Pan H, Peto R, Henao-Restrepo AM, Preziosi MP, Sathiyamoorthy V, et al. Repurposed antiviral drugs for Covid-19 — Interim WHO solidarity trial results. N. Engl. J. Med. 2021; 384: 497-511
6. Liu W, Li H COVID-19: Attacks the 1-beta chain of hemoglobin and captures the porphyrin to inhibit human heme metabolism. ChemRxiv 2020. doi: 10.26434/chem rxiv.11938173.v6
7. Cavezzi A, Troiani E, Corrao S COVID-19: hemoglobin, iron, and hypoxia beyond inflammation. A narrative review. Clin Pract 2020;10: 1271.
8. Munster VJ, Feldmann F, Williamson BN, van Doremalen N, Pérez-Pérez L, Schulz J, et al. Respiratory disease in rhesus macaques inoculated with SARS-CoV-2. Nature 2020; 585: 268-72.
9. Foy BH, Carlson JCT, Reinertsen E, Valls RPI, Lopez RP, Palanques-Tost E, et al. Association of red blood cell distribution width with mortality risk in hospitalized adults with SARS-CoV-2 infection. JAMA Netw. 2020; 3: e2022058.

10. Shah A, Frost JN, Aaron L, Donovan K, Drakesmith H, Collaborators, et al. Systemic hypoferremia and severity of hypoxemic respiratory failure in COVID-19. Critical Care 2020; 24: 320.
11. Ponka P Cell biology of heme. Am J Med Sci 1999;318: 241-56.
12. Faller M, Matsunaga M, Yin S, Loo JA, Guo F Heme is involved in microRNA processing. Nat Struct Mol Biol 2007; 14: 23-9.
13. Kumar S, Bandyopadhyay U Free heme toxicity and its detoxification systems in human. Toxicol Lett 2005; 157: 175-88.
14. Wagener FA, Volk HD, Willis D, Abraham NG, Soares MP, Adema GJ, et al. Different faces of the heme-heme oxygenase system in inflammation. Pharmacol Rev 2003; 55: 551–71.
15. de Souza GR, Hounkpe BW, Fiusa MML, Colella MP, Annichino-Bizzacchi JM, Traina F et al. Tissue factor-dependent coagulation activation by heme: A thromboelastometry study. PLoS One 2017; 12: e0176505.
16. Guo H, Pan X, Mao R, Zhang X, Wang L, Lu X, et al. Alkylated porphyrins have broad antiviral activity against hepadnaviruses, flaviviruses, filoviruses, and arenaviruses. Antimicrob Agents Chemother 2011; 55, 478-86.
17. Neris RLS, Figueiredo CM, Higa LM, Araujo DF, Carvalho CAM, Verçoza BRF, et al. Co-protoporphyrin IX and Sn-protoporphyrin IX inactivate Zika, Chikungunya and other arboviruses by targeting the viral envelope. Sci Rep 2018; 8: 9805.
18. Vzorov AN, Dixon DW, Trommel JS, Marzilli LG, Compans, RW Inactivation of human immunodeficiency virus type 1 by porphyrins. Antimicrob. Agents Chemother 2002; 46: 3917-25.
19. Gu C, Wu Y, Guo H, Zhu Y, Xu W, Wang Y, et al. Protoporphyrin IX and verteporfin potently inhibit SARS-CoV-2 infection in vitro and in a mouse model expressing human ACE2. Sci Bull (Beijing) 2020; Dec 9 doi: 10.1016/ j.scib.2020.12.005.
20. Yuki K, Fujiogi M, Koutsogiannaki S COVID-19 pathophysiology: A review. Clin Immunol 2020; 215: 108427.
21. Lazarian G, Quinquenel A, Bellal M, Siavellis J, Jacquy C, Re D, et al. Autoimmune haemolytic anaemia associated with COVID-19 infection. British J Haematol 2020; 190: 29-31.
22. Prieto-Pérez L, Fortes J, Soto C, Vidal-González Á, Alonso-Riaño M, Lafarga M, et al. Histiocytic hyperplasia with hemophagocytosis and acute alveolar damage in COVID-19 infection. Mod Pathol 2020; 33: 2139-46.
23. Litvinov RI, Weisel JW Role of red blood cells in haemostasis and thrombosis. ISBT Sci Ser 2017; 12: 176-183.
24. Dutra FF, Bozza, MT Heme on innate immunity and inflammation. Front Pharmacol 2014; 5, 115.
25. Li T, Bonkovsky HL, Guo J Structural analysis of heme proteins: implications for design and prediction. BMC Struct Biol 2011; 11: 13.
26. Wißbrock A, George AAP, Brewitz HH, Kühl T, Imhof D The molecular basis of transient heme-protein interactions: Analysis, concept and implementation. Biosci Rep 2019; 39: BSR20181940.
27. Zeng W, Liu G, Ma H, Zhao D, Yang Y, Liu M, et al. Biochemical characterization of SARS-CoV-2 nucleocapsid protein. Biochem Biophys Res Commun 2020; 527: 618-23.

816 28. Mense SM, Zhang L Heme: A versatile signaling molecule controlling the activities
817 of diverse regulators ranging from transcription factors to MAP kinases. Cell Res 2006;
818 16: 681-92.
819 29. Gordon DE, Jang GM, Bouhaddou M, Xu J, Obernier K, White KM, et al. A SARS-CoV-2
820 protein interaction map reveals targets for drug repurposing. Nature 2020; 583: 459-68.
821 30. Méndez R, De Haro C Casein kinase II is implicated in the regulation of heme-
822 controlled translational inhibitor of reticulocyte lysates. J Biol Chem 1994; 269: 617 0-6.
823 31. Han AP, Yu C, Lu L, Fujiwara Y, Browne C, Chin G, et al. Heme-regulated eIF2α kinase
824 (HRI) is required for translational regulation and survival of erythroid precursors in iron
825 deficiency. EMBO J 2001; 20: 6909-18.
826 32. Liu Y, Rutardottir S, Rajabi M, Wester Rosenlöf L, Alayash AI, Åkerström B. et al. The
827 role of host eIF2α in viral infection. Virology J 2020; 17: 112.
828 33. Karnaukhova E, Rutardottir S, Rajabi M, Wester Rosenlöf L, Alayash AI, Åkerström B
829 Characterization of heme binding to recombinant α1-microglobulin. Front Physiol 2014;
830 5: 465.
831 34. Ying W, Hao Y, Zhang Y, Peng W, Qin E, Cai Y, et al. Proteomic analysis on structural
832 proteins of severe acute respiratory syndrome coronavirus. Proteomics 2004; 4: 492-504.
833 35. Zeng R, Ruan HQ, Jiang XS, Zhou H, Shi L, Zhang L, et al. Proteomic analysis of SARS
834 associated coronavirus using two-dimensional liquid chromatography mass
835 spectrometry and one-dimensional sodium dodecyl sulfate-polyacrylamide gel
836 electrophoresis followed by mass spectrometric analysis. J Proteome Res 2004; 3: 549-55.
837 36. Pellitteri-Hahn MC, Warren MC, Didier DN, Winkler EL, Mirza SP, Greene AS et al.
838 Improved mass spectrometric proteomic profiling of the secretome of rat vascular
839 endothelial cells. J. Proteome Res.2006; 5: 2861-4.
840 37. Kumar A, Kumar P, Garg N, Giri R An insight into SARS-CoV-2 membrane protein
841 interaction with spike, envelope, and nucleocapsid proteins. Preprint 2020 at:
842 https://www.biorxiv.org/content/10.1101/2020.10.30.36300 2v1.
843 38. He R, Leeson A, Ballantine M, Andonov A, Baker L, Dobie F, et al. Characterization of
844 protein-protein interactions between the nucleocapsid protein and membrane protein of
845 the SARS coronavirus. Virus Res 2004;105: 121-5.
846 39. Dai L, Gao GF Viral targets for vaccines against COVID-19. Nat Rev Immunol 2021; 21:
847 73-82.
848 40. Guruprasad L Human SARS CoV-2 spike protein mutations. Proteins 2021; 89: 569-76.
849 41. Taneri PE, Gómez-Ochoa SA, Llanaj E, Raguindin PF, Rojas LZ, Roa-Díaz ZM, et al.
850 Anemia and iron metabolism in COVID-19: a systematic review and meta-analysis. Eur
851 J Epidemiol 2020; 35: 763-73.
852 42. Prayag S, Sarangi B, Shankar GH, Reddy VS, Walimbe A, Sharma V, et al. Mechanisms
853 of hypoxia in COVID-19 patients: A pathophysiologic reflection. Indian J Crit Care Med
854 2020; 24: 967-70.
855 43. Orino K, Lehman L, Tsuji Y, Ayaki H, Torti SV, Torti FM Ferritin and the response to
856 oxidative stress. Biochem J 2001; 357: 241-7.
857 44. Sonnweber T, Boehm A, Sahanic S, Pizzini A, Aichner M, Sonnweber B, et al. Persisting
858 alterations of iron homeostasis in COVID-19 are associated with non-resolving lung
859 pathologies and poor patients' performance: a prospective observational cohort study.
860 Respir Res 2020; 21: 276.
861 45. Weisel JW, Litvinov RI Red blood cells: the forgotten player in hemostasis and
862 thrombosis. J Thromb Haemost 2019; 17: 271-82.

46. Janz DR, Ware LB The role of red blood cells and cell-free hemoglobin in the pathogenesis of ARDS. J Intensive Care 2015; 3: 20.
47. Mumby S, Ramakrishnan L, Evans TW, Griffiths MJD, Quinlan GJ Methemoglobin-induced signaling and chemokine responses in human alveolar epithelial cells. Am J Physiol Lung Cell Mol Physiol 2014; 306: L88-100.
48. Stojiljkovic I, Evavold BD, Kumar V Antimicrobial properties of porphyrins. Exp. Op. Inv. Drugs 2001; 10: 309-20.
49. Simoni J, Simoni G, Moeller, JF (Intrinsic toxicity of hemoglobin: How to counteract it. Artif Organs. 2009; 33: 100-9.
50. Zhang A, Wan B, Jiang D, Wu Y, Ji P, Du Y, et al. The cytoprotective enzyme heme oxygenase-1 suppresses pseudorabies virus replication in vitro. Front Microbiol 2020; 11: 412.
51. Protzer U, Seyfried S, Quasdorff M, Sass G, Svorcova M, Webb D, et al. Antiviral activity and hepatoprotection by heme oxygenase-1 in Hepatitis B virus infection. Gastroenterology 2007; 133: 1156-65.
52. Lehmann E, El-Tantawy WH, Ocker M, Bartenschlager R, Lohmann V, Hashemolhosseini S, et al. The heme oxygenase 1 product biliverdin interferes with hepatitis C virus replication by increasing antiviral interferon response. Hepatology 2010; 51: 398-404.
53. Sass G, Seyfried S, Soares MP, Yamashita K, Kaczmarek E, Neuhuber WL, et al. Cooperative effect of biliverdin and carbon monoxide on survival of mice in immune-mediated liver injury. Hepatology 2004; 40: 1128-35.
54. Hashiba, T. et al. Adenovirus-mediated transfer of heme oxygenase-1 cDNA attenuates severe lung injury induced by the influenza virus in mice. Gene Ther 2001; 8: 1499-507
55. Milburn D, Laskowski RA, Thornton JM Sequences annotated by structure: A tool to facilitate the use of structural information in sequence analysis. Protein Eng 1998; 11 855-9.
56. Espinoza JA, León MA, Céspedes PF, Gómez RS, Canedo-Marroquín G, Riquelme SA, et al. Heme oxygenase-1 modulates human respiratory syncytial virus replication and lung pathogenesis during infection. J Immunol 2017; 199: 212-23.
57. El Kalamouni C, Frumence E, Bos S, Turpin J, Nativel B, Harrabi W, et al. Subversion of the heme oxygenase-1 antiviral activity by zika virus. Viruses 2019; 11: 2
58. Bailey TL, Boden M, Buske FA, Frith M, Grant CE, Clementi L, et al. MEME Suite: Tools for motif discovery and searching. Nucleic Acids Res 2009; 37: W202-8.
59. CDC. Real-time RT-PCR Primers and Probes for COVID-19|CDC. Available at:https://www.cdc.gov/coronavirus/2019-ncov/lab/rt-pcr-panel-primer-pro bes. html. (Accessed: March 25 2021)
60. Dias SSG, Soares VC, Ferreira AC, Sacramento CQ, Fintelman-Rodrigues N, Temerozo JR, et al. Lipid droplets fuel SARS-CoV-2 replication and production of inflammatory mediators. PLoS Pathog. 2020; 16: e10091 27.
61. Laemmli UK Cleavage of structural proteins during the assembly of the head of bacteriophage T4. Nature 1970; 227: 680-5.
62. Yuan X, Rietzschel N, Kwon H, Nuno ABW, Hanna DA, Phillips JD, et al. Regulation of intracellular heme trafficking revealed by subcellular reporters. Proc Natl Acad Sci USA 2016; 113: E5144-52.

908 63. Zhou JR, Bu DR, Zhao XF , Wu F, Chen XQ, Shi HZ, et al. Hc-hrg-2, a glutathione
909 transferase gene, regulates heme homeostasis in the blood-feeding parasitic nematode
910 *Haemonchus contortus*. Parasit Vectors 2020; 13: 40.
911 64. Mbanefo EC, Kikuchi M, Huy NT , Shuaibu MN, Cherif MS, Yu C et al. Characterization
912 of a gene family encoding sea (sea-urchin sperm protein, enterokinase and agrin)-
913 domain proteins with lectin-like and heme-binding properties from *Schistosoma*
914 *japonicum*. PLoS Negl Trop Dis 2014; 8: e2644.
915 65. De-Simone SG, Napoleão-Pêgo P, De-Simone TS Spot Synthesis: An optimized
916 microarray to detect IgE epitopes. Methods Mol. Biol. 2016;1352: 263-77.
917 66. De-Simone SG, Gomes LR, Napoleão-Pêgo P, Lechuga GC. Pina JC, Silva FR
918 Identification of linear B epitopes liable for the protective immunity of diphtheria toxin.
919 Vaccines 2021; 9: 313.
920 67. Wilm M, Shevchenko A, Houthaeve T, Breit S, Schweigerer L, Fotsis T, et al. Femtomole
921 sequencing of proteins from polyacrylamide gels by nano electrospray mass
922 spectrometry. Nature 1996; 379: 466-9.
923 68. Basto VLFC, Salles JB, Valente RH, León IR, Perales J, Dantas RF, et al. Cytosolic
924 glutathione peroxidase from liver of pacu (*Piaractus mesopotamicus),* a hypoxia-tolerant
925 fish of the Pantanal. Biochimie 2007; 89: 1332-42.

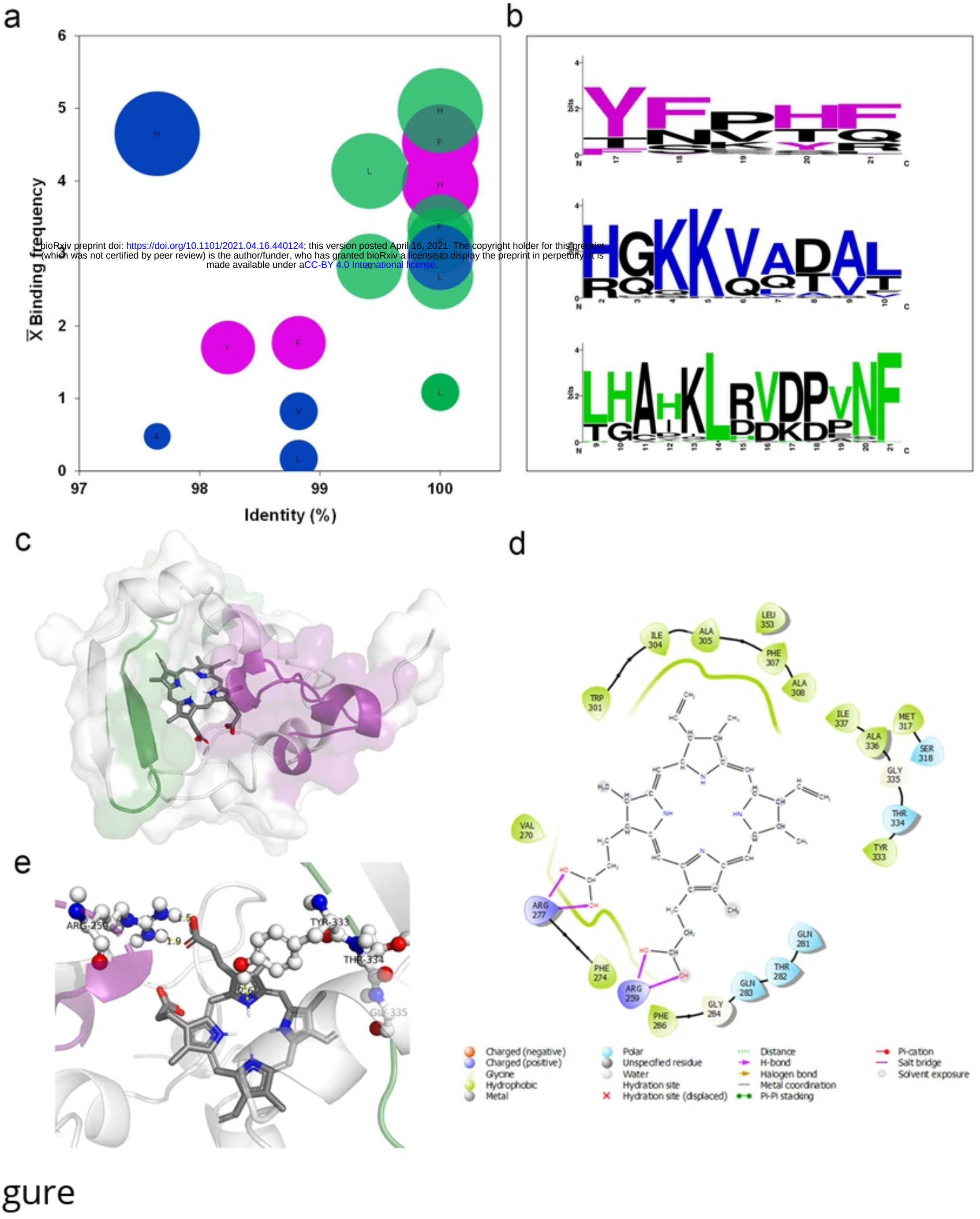

Figure

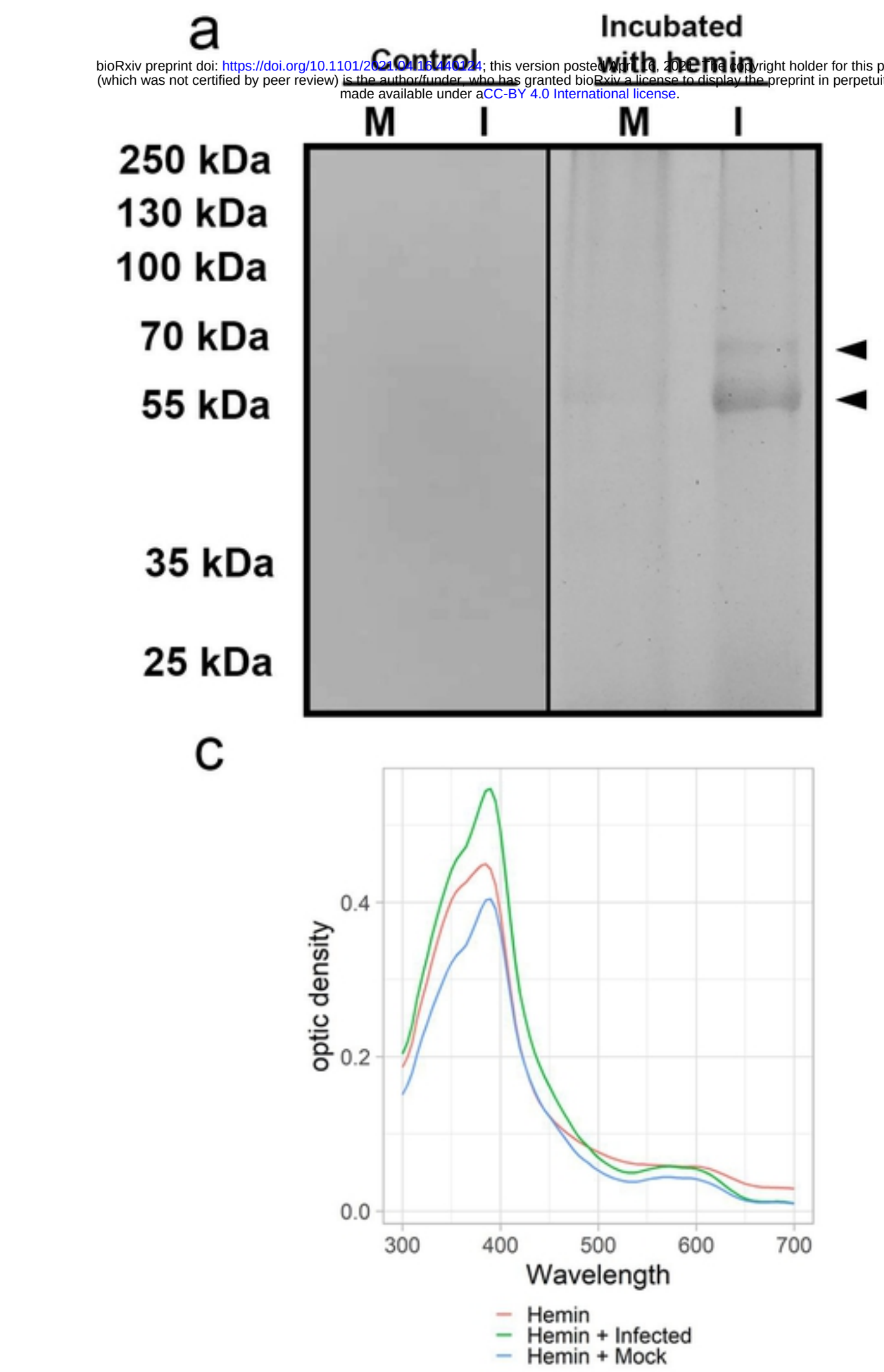

Figure

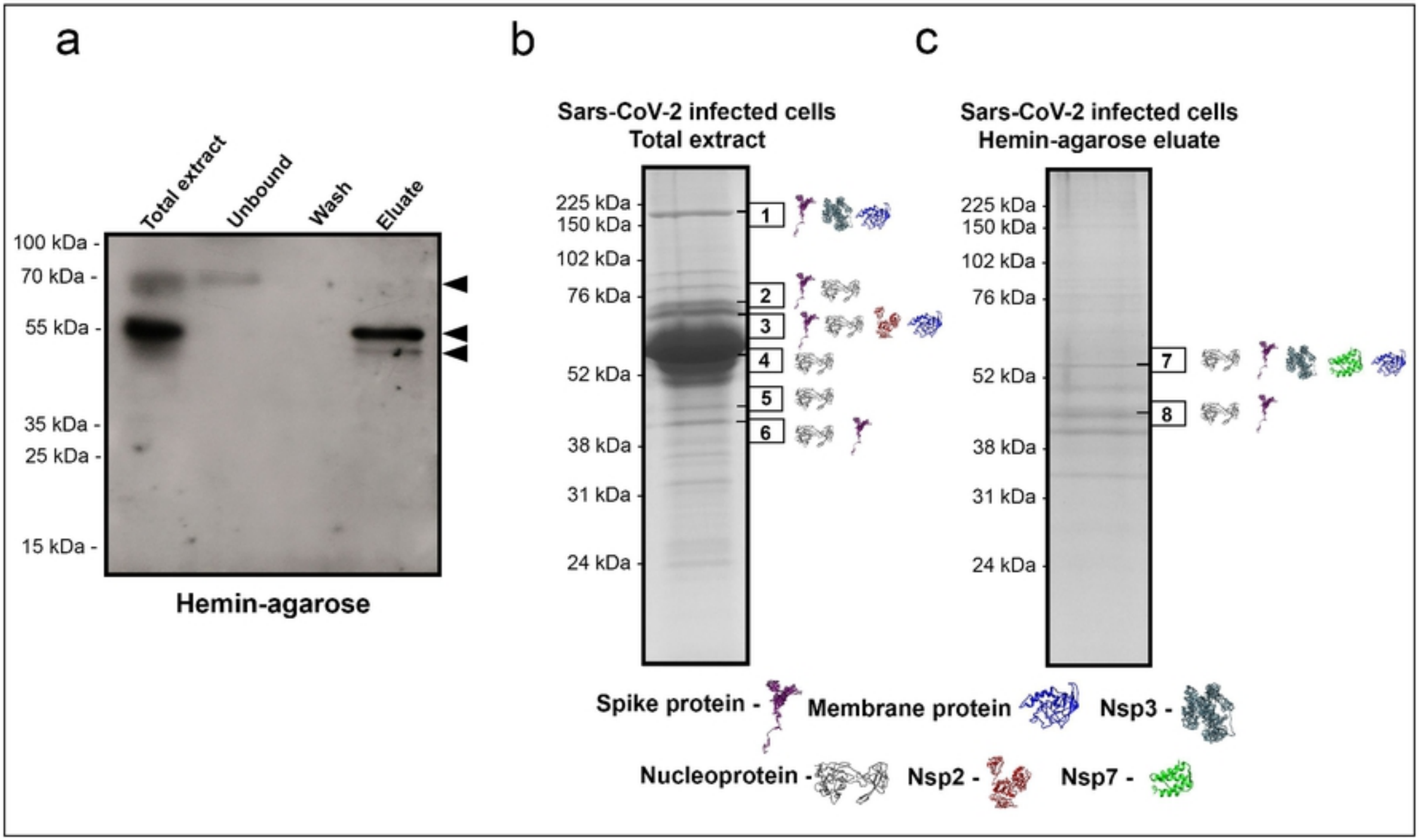
a
Total extract
Unbound
Wash
Eluate
100 kDa -
70 kDa -
55 kDa -
35 kDa -
25 kDa -
15 kDa -
Hemin-agarose
b
Sars-CoV-2 infected cells
Total extract
225 kDa
150 kDa
102 kDa
76 kDa
52 kDa
38 kDa
31 kDa
24 kDa
1
2
3
4
5
6
c
Sars-CoV-2 infected cells
Hemin-agarose eluate
225 kDa
150 kDa
102 kDa
76 kDa
52 kDa
38 kDa
31 kDa
24 kDa
7
8
Spike protein -
Membrane protein
Nsp3 -
Nucleoprotein -
Nsp2 -
Nsp7 -

Figure

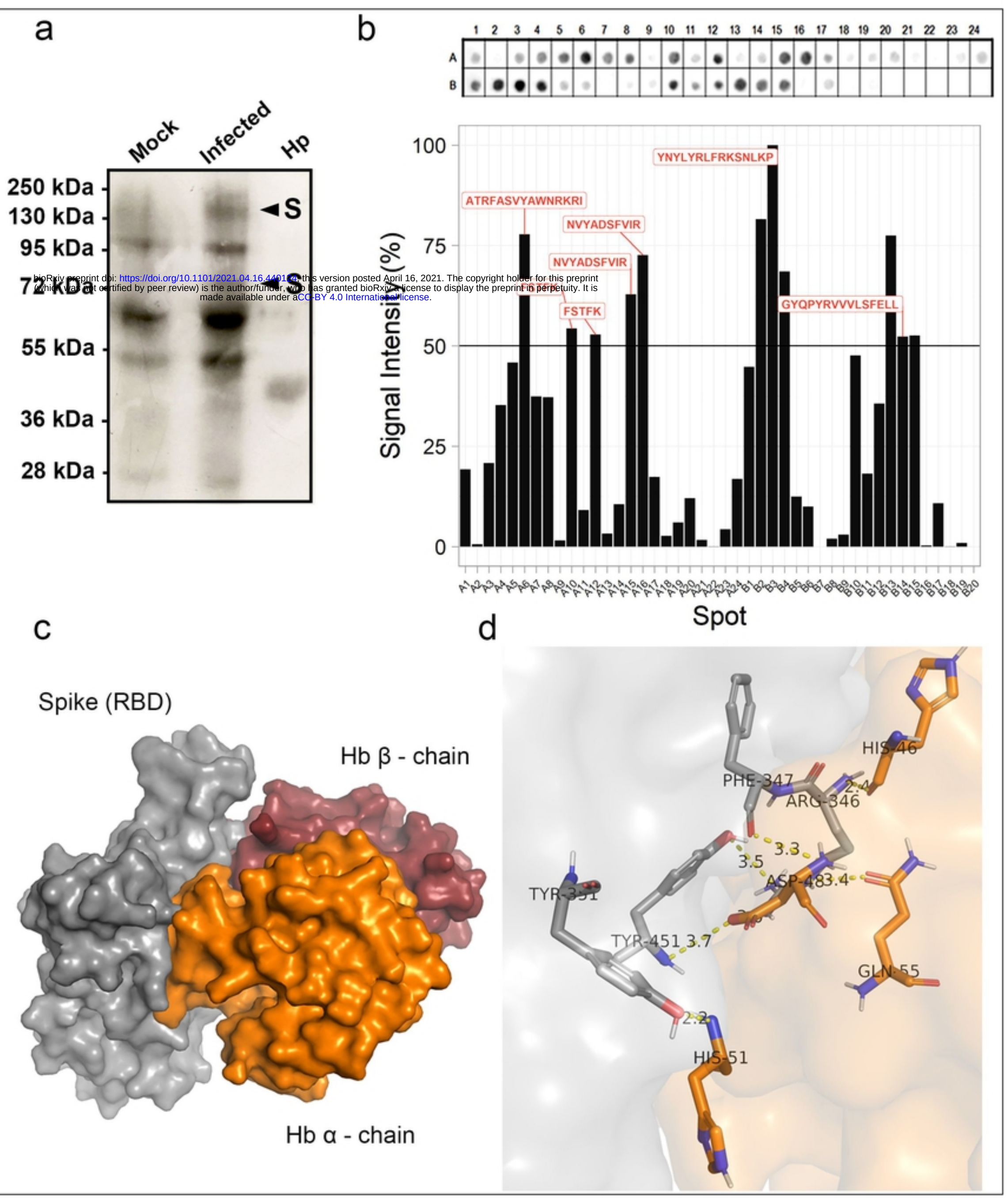

Figure

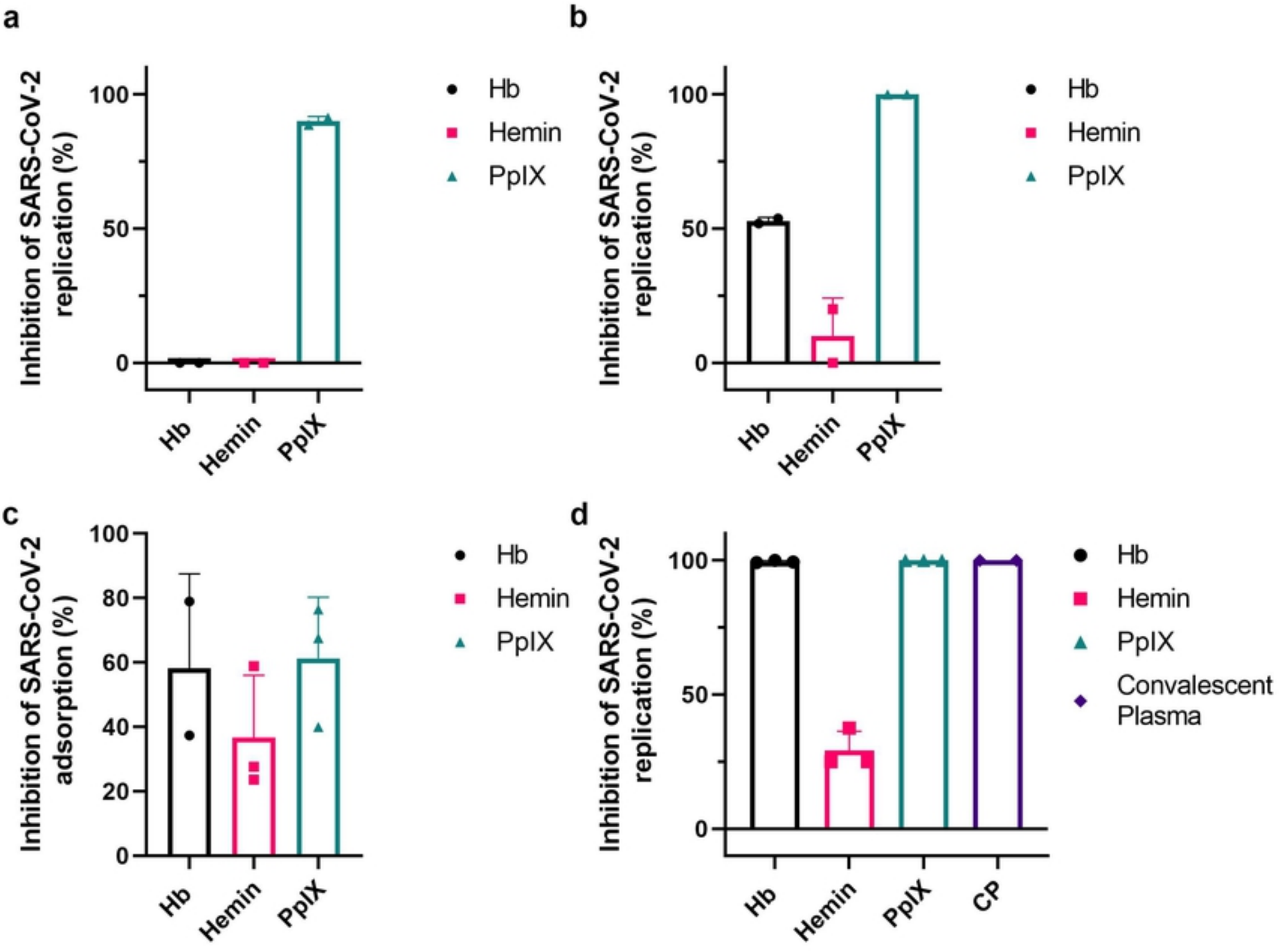
a
Inhibition of SARS-CoV-2 replication (%)
100
50
0
Hb
Hemin
PpIX
Hb
Hemin
PpIX
b
Inhibition of SARS-CoV-2 replication (%)
100
50
0
Hb
Hemin
PpIX
Hb
Hemin
PpIX
c
Inhibition of SARS-CoV-2 adsorption (%)
100
80
60
40
20
0
Hb
Hemin
PpIX
Hb
Hemin
PpIX
d
Inhibition of SARS-CoV-2 replication (%)
100
50
0
Hb
Hemin
PpIX
CP
Hb
Hemin
PpIX
Convalescent Plasma

Figure

HEME binding proteins (PDB Code)	Hemoglobin human (Uniprot Code)	Nucleoprotein Sars-CoV (Uniprot Code)
1a00:A	P02008	NCAP_SARS
1a3o:A	P02042	A0A679GC99_SARS2
1bz1:A	P02100	A0A6H2EFU6_SARS2
1bzz:A	P69892	A0A6G8I2S4_SARS2
1c0h:A	P68871	A0A6H1PLH4_SARS2
1c7d:A	P69905	NCAP_SARS2
1dhb:A	Q9NZD4	A0A6C0T6Z7_SARS2
1dsh:A	P09105	A0A6C0N5E8_SARS2
1fhj:A	Q6B0K9	A0A6H2L5M8_SARS2
1hbr:A	Q1W6G9	A0A6B9VLF5_SARS2
1hda:A	A0A1K0GXZ1	A0A6C0WXA2_SARS2
1hbs:A	C1MGQ2	A0A6H0MAP2_SARS2
1ibe:A	A0A1K0GUV5	A0A6H1PIQ7_SARS2
1j7s:A	U6A216	
1mhb:A	A0A2R8Y7C0	
1ns6:A	A0A1S5UZ39	
1o1k:A	A0A385HVZ2	
1o1l:A	A0A385HW21	
1o1m:A	A0A385HW02	
1o1n:A	Q6J1Z9	
1o1o:A	Q86YQ1	
1o1p:A	A0A385HVY8	
1pgh:A	A0A385HW00	
1s0h:A	A0A0K2BMD8	
1v75:A	Q86YL2	
1xy0:A	I1VZV6	
1xye:A	Q9BX83	
1xz5:A	E9M4D4	
1xz7:A	Q9NQT3	
1xzu:A	Q96T46	
1xzv:A	E1B2D1	
1y09:A	Q86YQ4	
1y0a:A	E9LUX2	
1y0c:A	V9H1D9	
1z8u:B	P78461	
2dhb:A	Q4ZGM8	
2mhb:A		
2pgh:A		
2qls:A		
2qsp:A		
2qu0:A		
2ri4:A		
2zfb:A		
2zlt:A		
2zlu:A		
3a59:A		
3at5:A		
3cy5:A		
3d4x:A		
3dht:A		
3eok:A		

3gdj:A
3gou:A
3gys:A

The search returned 399 sequences with motifs HEME binding, but only 68 structures present complexes only with the HEME group.

Protein	Residue	Complex ASA[b]	Monomer ASA[b]	Pair Potential	Hotspot Status [a]	Hotregion Status	Complex ASA[b]	Monomer ASA[b]
HB_A	LEU35	26.04	73.04	17.36	NH		46.51	130.4
HB_A	PRO38	42.98	61.77	2.43	NH		58.51	84.09
HB_A	LYS41	0	0	13.92	NH		0	0
HB_A	HIS42	0	0	5	NH		0	0
HB_A	PRO45	0	0	4.99	NH		0	0
HB_A	HIS46	0	0	9.17	NH		0	0
HB_A	PHE47	0	0	14.04	NH		0	0
HB_A	ASP48	0	0	19.97	H	2	0	0
HB_A	SER50	0	0	17.74	NH		0	0
HB_A	HIS51	0	0	19.4	H	-	0	0
HB_A	GLY52	0	0	11.09	NH		0	0
HB_A	SER53	0	0	7.25	NH		0	0
HB_A	ALA54	0	0	7.56	NH		0	0
HB_A	GLN55	0	0	12.46	NH		0	0
RBD_C	GLU340	47.25	67.63	7.68	NH		81.38	116.5
RBD_C	ALA344	0	0	7.56	NH		0	0
RBD_C	THR345	0	0	6.17	NH		0	0
RBD_C	ARG346	0	0	27.67	H	2	0	0
RBD_C	PHE347	0	0	22.7	H	2	0	0
RBD_C	ALA348	0	0	17.73	NH		0	0
RBD_C	SER349	0	0	12.03	NH		0	0
RBD_C	TYR351	0	0	24.76	H	-	0	0
RBD_C	ALA352	0	0	16.19	NH		0	0

RBD_C	TRP353	0	0	16.59	NH		0	0
RBD_C	ASN354	0	0	10.77	NH		0	0
RBD_C	ARG355	0	0	15.53	NH		0	0
RBD_C	ASN450	0	0	13.12	NH		0	0
RBD_C	TYR451	0	0	31.74	H	1	0	0
RBD_C	LEU452	0	0	33.83	H	1	0	0
RBD_C	ARG466	26.46	58.18	12.34	NH		63.18	138.9
RBD_C	ILE468	22.38	56.43	10.14	NH		39.11	98.82
RBD_C	LEU492	0	0	22.69	H	1	0	0

[a] NH denotes non hot spot and H denotes hot spot and [b] Solvent Accessible Surface Area (ASA)

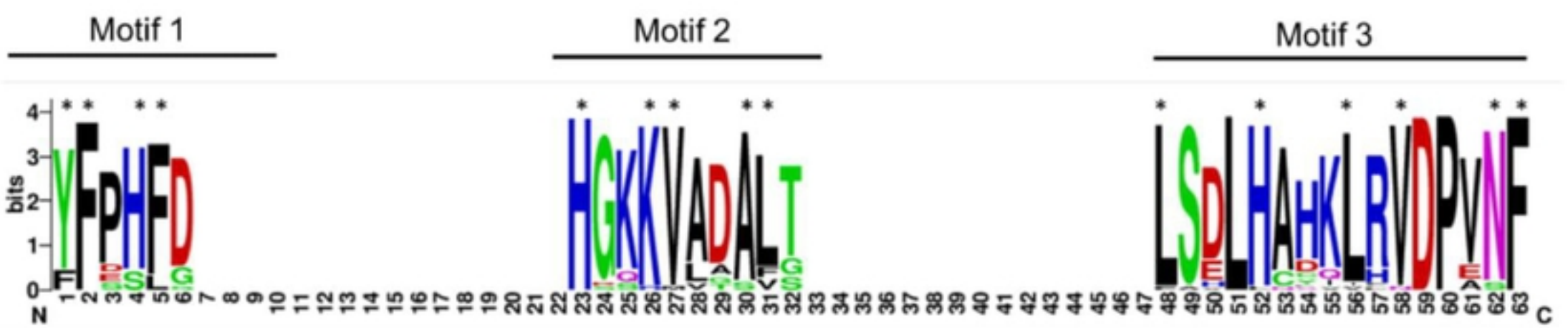

Motifs	p-value	q-value
YFPHFD	1.2×10^{-12}	3.7×10^{-6}
HGKKVADALT	4.2×10^{-13}	1.3×10^{-6}
LSDLHAHKLRVDPVNF	8.4×10^{-21}	2.5×10^{-14}

Figure Supplementary

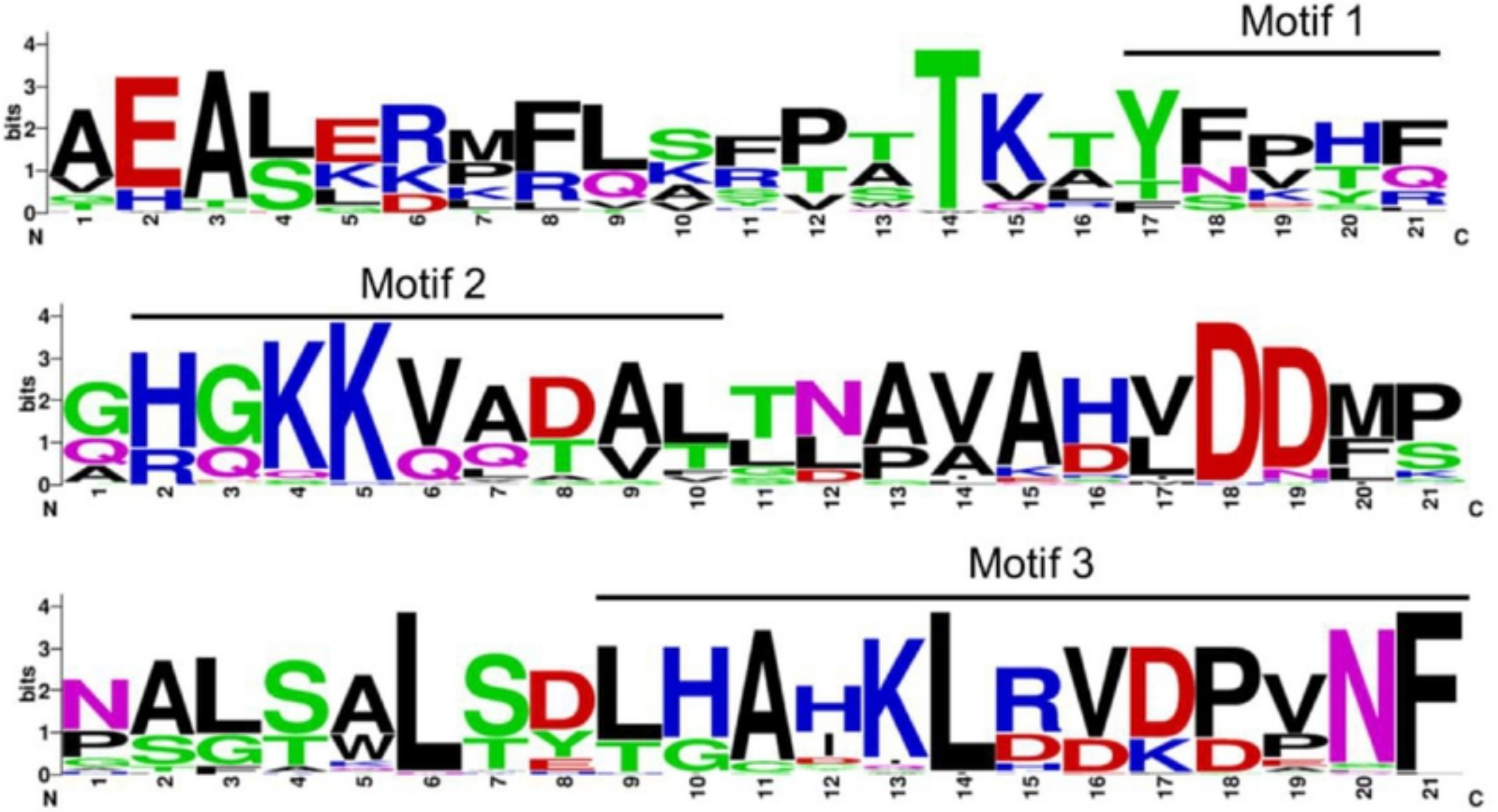

Figure Supplementary

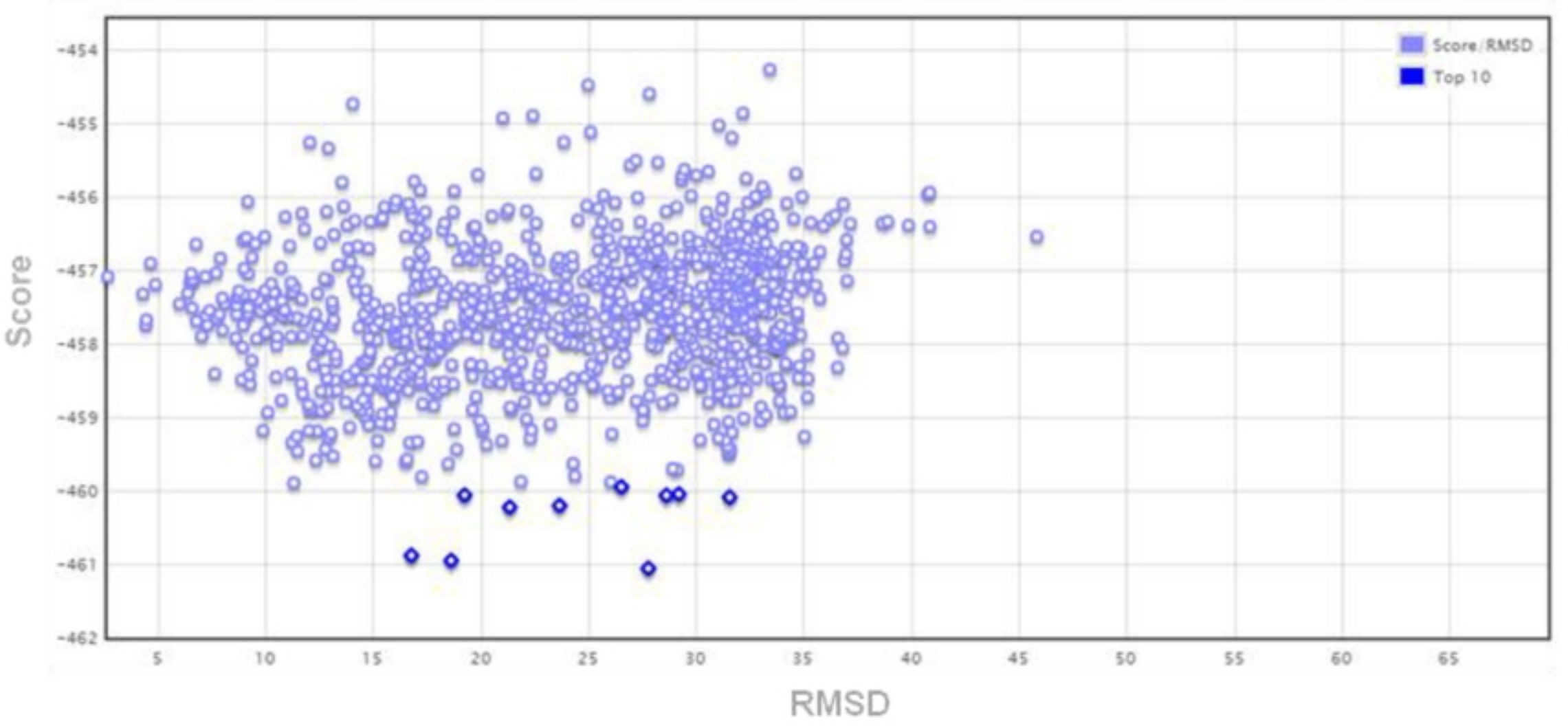

Figure Supplementary